

Roles of air-sea coupling and horizontal resolution in the climate model simulation of Indian monsoon low pressure systems

Article

Accepted Version

Levine, R. C., Klingaman, N. P. ORCID: <https://orcid.org/0000-0002-2927-9303>, Peatman, S. and Martin, G. M. (2021) Roles of air-sea coupling and horizontal resolution in the climate model simulation of Indian monsoon low pressure systems. *Climate Dynamics*, 56. pp. 1203-1226. ISSN 0930-7575 doi: <https://doi.org/10.1007/s00382-020-05526-6> Available at <https://centaur.reading.ac.uk/93808/>

It is advisable to refer to the publisher's version if you intend to cite from the work. See [Guidance on citing](#).

To link to this article DOI: <http://dx.doi.org/10.1007/s00382-020-05526-6>

Publisher: Springer

All outputs in CentAUR are protected by Intellectual Property Rights law, including copyright law. Copyright and IPR is retained by the creators or other copyright holders. Terms and conditions for use of this material are defined in the [End User Agreement](#).

www.reading.ac.uk/centaur

CentAUR

Central Archive at the University of Reading

Reading's research outputs online

Roles of air-sea coupling and horizontal resolution in the climate model simulation of Indian monsoon low pressure systems

Richard C. Levine · Nicholas P. Klingaman · Simon C. Peatman · Gill M. Martin

the date of receipt and acceptance should be inserted later

Received: date / Accepted: date

Abstract The roles of air-sea coupling and horizontal resolution in the representation of Indian monsoon low pressure systems (LPS) in Met Office Unified Model (MetUM) global climate simulations are investigated. To avoid the generally large sea surface temperature (SST) biases in standard coupled atmosphere-ocean global climate models (GCMs), the analysis is performed on experiments from an atmosphere model coupled to a mixed-layer ocean model (MetUM-GOML2), which allows coupling to be applied regionally as well as globally, while constraining the ocean mean state in coupled regions. Compared to the standard AMIP-style MetUM atmosphere-only simulations, the MetUM-GOML2 simulations produce more monsoon LPS, which is attributed to effects of relatively small remaining (Indian Ocean) SST biases that somewhat strengthen the atmospheric monsoon base state. However, the MetUM-GOML2 simulations, all starting from the same atmospheric and oceanic base state, allow for an idealised approach to evaluate the relative effects of coupling and resolution. When the effects of SST biases are excluded, global coupling has a neutral impact on the number of LPS formed, while the associated rainfall is somewhat reduced due to a local negative air-sea feedback reducing the strength of atmospheric convection and weakening individual LPS. The MetUM-GOML2 simulations show particular sensitivity to localised coupling in the In-

dian and Pacific Oceans, which appears to enhance the effect of monsoon LPS. Although, in contrast to the global coupling comparison, the comparison of regionally coupled simulations is affected by both differences in interannual SST variability and SST biases, and it is likely that this causes at least part of the positive effects from Indian and Pacific Ocean coupling. More importantly, however, is that the effects of air-sea coupling are substantially smaller than the positive effects of the increase in horizontal resolution from N96 (approx. 200km) to N216 (approx. 90km). The resolution effect is also larger than that seen in older MetUM configurations.

Keywords Indian Monsoon · Global Climate Model · Low Pressure Systems · Air-sea coupling · Horizontal resolution

1 Introduction

Air-sea coupling and horizontal resolution are generally considered important for accurate simulations of climate and its components, for example the South Asian Summer Monsoon (SASM). In this paper the hypothesis is tested that they are important for synoptic-scale monsoon depressions and lows, which are important phenomena of the SASM. These systems contribute substantially to seasonal rainfall totals over the Indian subcontinent, while also causing many of the extreme rainfall events during the summer monsoon season (Sikka 1977; Krishnamurthy and Ajayamohan 2010; Praveen et al. 2015; Hunt et al. 2016); therefore their realistic representation is essential for climate predictions and projections on a range of time-scales.

The simulation of monsoon LPS in current climate models is often poor (Ashok et al. 2000; Sabre et al.

Richard C. Levine · Gill M. Martin
Met Office Hadley Centre
Exeter, UK
E-mail: richard.levine@metoffice.gov.uk

Nicholas P. Klingaman · Simon C. Peatman
National Centre for Atmospheric Science-Climate
Department of Meteorology
University of Reading, Reading, UK

2000; Stowasser et al. 2009; Praveen et al. 2015; Levine and Martin 2018), with a deficient number of LPS and associated rainfall. In atmosphere-only models this may relate to the lack of air-sea coupling, which is important in other aspects of monsoon variability (as discussed below), or to coarse horizontal resolution. An increase in horizontal resolution may provide finer-scale detail that may help to improve the organization and propagation of LPS. However, including air-sea coupling and increasing resolution also substantially increase the complexity and expense of climate model simulations, therefore it is important to understand their individual effects.

Air-sea coupling is important in determining the formation, intensity and pathway of (Indian Ocean) tropical cyclones in climate models (eg. Subrahmanyam et al. 2005). It has also been shown to be important for the climate-model simulation of monsoon interannual variability (eg. Shukla and Huang 2016 and references therein) and intra-seasonal variability, including the onset vortex (Wu et al. 2012). Air-sea coupling and intra-seasonal sea surface temperature (SST) variability support the northward propagation of the boreal summer intra-seasonal oscillation (BSISO) that is associated with monsoon active-break cycles (Fu and Wang, 2004; DeMott et al. 2014), with coupling resulting in improvements to the relationship between SST and atmospheric convection, and contributes via the effect of high-frequency SST variability on surface fluxes to an estimated 20 % of the propagation of convection that is involved in the northward component of the BSISO (Gao et al. 2019). The prevalence and strength of monsoon depressions is highly correlated with active-break cycles (Krishnamurthy and Shukla, 2007), which suggests air-sea coupling may be important for the simulation of LPS, which often form, intensify and propagate over the warm summer Bay of Bengal (BoB) SSTs (Sikka 1977). Air-sea coupling may also reduce the intensity of monsoon LPS, due to local negative thermodynamic feedbacks on atmospheric convection that have been found to reduce extreme rainfall over the tropics in a similar coupled modelling setup as used in this study (Hirons et al. 2018). These feedbacks weaken local intense convection via reducing atmosphere-to-ocean net surface heat fluxes and increasing near-surface wind speeds, which cool the SST, reduce latent and sensible heat fluxes, and thereby weaken convection.

Coupled atmosphere-ocean configurations of the Met Office Unified Model (MetUM) generally show an increase in LPS over their atmosphere-only equivalents. However, the realistic effects of air-sea coupling alone are difficult to establish due to the development of substantial SST biases in coupled climate models, which

are especially wide-spread over the northern and equatorial Indian Ocean, both of which substantially affect the mean state atmospheric monsoon (Levine et al. 2013; Levine and Turner 2012; Bollasina and Ming 2013; Bollasina and Nigam 2009), thereby highlighting the importance of correctly representing air-sea coupled feedbacks. Coupled model SST biases have also been shown to negatively affect tropical sub-seasonal variability, including the Madden-Julian Oscillation (MJO) (Klingaman and Woolnough (2014), DeMott et al. 2015) and tropical cyclones (eg. Hsu et al. 2019), and therefore may also impact monsoon LPS.

In order to minimise the effect of coupled model SST biases, new simulations are analyzed using a configuration of the MetUM atmosphere model coupled to many columns of a mixed-layer ocean (MetUM-GOML2), whereby ocean temperature and salinity, and therefore also SSTs, are constrained to an observed mean seasonal cycle via corrections (Hirons et al. 2015). Furthermore, the one-dimensional ocean model allows air-sea coupling to be applied globally or in specific regions, allowing separation of the contributions from local and remote air-sea interactions to the representation of monsoon LPS. A further key advantage is that when the horizontal resolution of the ocean and atmosphere change, the oceanic mean state remains consistent, because the ocean mean state is constrained to observations by prescribed temperature and salinity corrections. This allows separation of the effects on monsoon LPS from changes to resolution, and from changes in the oceanic mean state. This is not possible in a fully coupled atmosphere-ocean model, where a change in resolution will also change the oceanic and atmospheric mean state.

Compared to a fully coupled atmosphere-ocean model, the MetUM-GOML2 model lacks ocean dynamics, an important factor in SST variability. However, on synoptic to sub-seasonal time-scales that are of interest to monsoon LPS, the SST variability over the Indian Ocean is largely controlled by thermodynamic processes (e.g., Halkides et al 2015). The technique of applying temperature and salinity corrections in MetUM-GOML2 could also be applied to a fully coupled atmosphere-ocean model, but the presence of interactive ocean dynamics can complicate the results as the ocean dynamical response may lead the ocean model to drift away from the desired ocean mean state. In MetUM-GOML2, the lack of an ocean dynamical feedback to the corrections allows the effective use of imposed fixed corrections. This method is not a relaxation; it is a prescribed seasonal cycle of correction terms that are obtained from an initial, separate relaxation simulation (which is not analysed in this study; see Hirons et al. 2015 for details).

168 These MetUM-GOML2 simulations have previously
169 been used by Peatman and Klingaman (2018) to inves-
170 tigate the influence of air-sea coupling and horizontal
171 resolution on the mean Indian summer monsoon and
172 its sub-seasonal variability. While coupling over the In-
173 dian Ocean degrades the atmospheric mean state due
174 to the presence of small remaining SST biases, there
175 are some improvements to the northward propagation
176 of the BSISO. Increasing the horizontal resolution from
177 200km to 90km improves the simulation of monsoon
178 rainfall and circulation, but there are no further im-
179 provements when the resolution is increased again to
180 40km. The improvements to the intra-seasonal variabil-
181 ity from increasing the resolution from 200km to 90km
182 are found to be of similar magnitude to the improve-
183 ments due to air-sea coupling over the Indian Ocean.

184 Previous work using an older version (Global At-
185 mosphere (GA) 3, described in Walters et al. 2011) of
186 the MetUM regional climate model (RCM) atmosphere-
187 only configuration suggested that the representation of
188 monsoon LPS can be substantially improved if biases in
189 the large-scale flow into the Indian monsoon area are
190 corrected (Levine and Martin 2018), while increasing
191 the horizontal resolution from 50km to 12km has lit-
192 tle effect (Karmacharya et al. 2016). Analysis of global
193 atmosphere-only model simulations at the same Me-
194 tUM version (GA3) has suggested little sensitivity of
195 monsoon LPS to increasing the horizontal resolution
196 from N96 (200km) up to N512 (40km) (Johnson et al.
197 2016). A newer version of the MetUM (GA6, described
198 in Walters et al. 2017), including the new dynamical
199 core ENDGAME, is used in this study, which may ex-
200 plain any difference in sensitivities.

201 While increased horizontal resolution may be ben-
202 efcial, as seen for example in analysis of monsoon de-
203 pression case studies in Numerical Weather Prediction
204 (NWP) simulations (Hunt and Turner 2017), the stud-
205 ies discussed above suggest that improving the overall
206 tropical circulation in the GCM at the standard hori-
207 zontal resolution would most improve our representa-
208 tion of monsoon LPS. In this case the improved repre-
209 sentation of mean SST and the monsoon circulation as
210 a whole in MetUM-GOML2 found with increased reso-
211 lution and air-sea coupling (Peatman and Klingaman,
212 2018) may benefit monsoon LPS as well. It is interest-
213 ing to note that in most MetUM GCM experiments,
214 and also in the general development cycle of the Me-
215 tUM GCM, the strength of the mean state atmospheric
216 monsoon circulation (and rainfall) is always positively
217 correlated with the number of LPS (and their associ-
218 ated rainfall), which is also supported by CMIP5 anal-
219 ysis (Praveen et al. 2015). Levine and Martin (2018)
220 suggest that a stronger mean monsoon would increase

monsoon LPS, while there may be a positive feedback
with more and stronger monsoon LPS strengthening
the larger-scale flow into the region.

This study aims to establish whether increasing hori-
zontal resolution, using a range typical of current GCMs,
and the inclusion of a simple form of air-sea coupling,
over an atmosphere-only model, improves the forma-
tion, trajectories and associated rainfall of monsoon
LPS.

2 Simulations and data

The simulations use the GA6 configuration of the Me-
tUM atmosphere model (Walters et al. 2017).

Atmosphere-only experiments forced with observed
SST use the AMIP methodology (Gates et al. 1998)
and are forced with daily SST and sea-ice fractions from
Reynolds et al. (2007). Fully coupled atmosphere-ocean
MetUM present day control simulations use the GC2
configuration (Williams et al. 2015).

The mixed-layer ocean coupling experiments use the
MetUM-GOML2 configuration (Hirons et al. 2015), where
the vertical profiles of ocean temperature and salinity
are constrained using a prescribed seasonal cycle of cor-
rections. For all MetUM-GOML2 simulations analysed
here, the ocean is constrained to the 1980-2009 clima-
tology from Met Office ocean analyses (Smith and Mur-
phy, 2007). The coupling can be applied selectively in
space, and thereby allows coupling in individual ocean
basins only without substantial changes to the ocean
mean state. The resulting coupled simulations thereby
minimize the effects of changes in mean SST on the
atmosphere, although they still contain small SST bi-
ases (typically less than $\pm 0.5^\circ\text{C}$, although locally can
be over $\pm 1.0^\circ\text{C}$; see Peatman and Klingaman (2018)).
Due to limitations with regard to sea-ice cover, the cou-
pling is applied over the approximate latitude band
of 60°S - 60°N (see Hirons et al. 2015, Figure 2). The
lack of ocean dynamics means there is no representa-
tion of El Nino Southern Oscillation (ENSO) or Indian
Ocean Dipole (IOD) variability in the ocean (Hirons
et al. 2015). An indication of intraseasonal variability
of SST in MetUM-GOML2 for 90km simulations (the
higher horizontal resolution used in this study) is shown
by Peatman and Klingaman (2018) (their Fig. 7). This
shows that MetUM-GOML2 underestimates intrasea-
sonal variability in most of the tropical Indian Ocean,
with the strongest biases on the equator and in the
Arabian Sea. These are both regions where ocean dy-
namics (upwelling) are important for SST variability. In
the BoB, where most LPSs form and intensify, biases in
intraseasonal SST variability are smaller and consistent
with those in fully coupled GCMs.

Further, we note that the SST variability in the free-running MetUM-GOML2 simulation analysed here does not depend on the nudging timescale applied in the initial relaxation simulation (which is not analysed in this study). The free-running MetUM-GOML2 coupled simulations are corrected only by the mean seasonal cycle of temperature and salinity corrections from the relaxation simulations. Because these are fixed corrections, not a relaxation, the corrections do not damp SST variability. Indeed, Hirons et al. (2015) noted that shortening the relaxation timescale would increase the mean bias in the free-running simulation.

Simulations at N96 (longitude x latitude: $1.875^\circ \times 1.25^\circ$, approximately 200km at equator) and N216 ($0.83^\circ \times 0.55^\circ$, approximately 90km at equator) horizontal resolutions are compared. The simulations analysed are summarised in Table 1, and the notation for the simulations is discussed in the caption. Where SSTs from coupled model simulations have been used to force atmosphere-only simulations a 31-day smoothing has first been applied, following recommendations from DeMott et al. (2015). In simulations where coupling is applied regionally, climatological monthly-varying SST from Met Office ocean analyses (Smith and Murphy, 2007) are prescribed outside the coupled region. This means it is necessary to take account of interannual SST variability that is not present in the uncoupled regions, but is present in the globally coupled simulation and atmosphere-only simulation forced with either observed SST or SST from the globally coupled simulation. It is important to emphasize that the coupled regions in the MetUM-GOML2 simulations do have interannual variability in SST, however, this does not organise into coupled modes like ENSO or the IOD.

The 31-day smoothing to coupled model SSTs is recommended by DeMott et al. (2015) as it has been found that applying high-frequency (e.g., daily) SST forcing in an atmosphere-only global climate model (AGCM) leads to erroneous feedbacks between surface fluxes, SSTs and convection that amplify the rainfall response to SSTs and complicate the analysis of synoptic and sub-seasonal variability. In particular, AGCM convection parametrisations respond strongly and quickly to SST variability, such that in an AGCM, high-frequency warm SST anomalies are collocated with enhanced surface fluxes and high precipitation; high-frequency cold SST anomalies are collocated with reduced surface fluxes and low precipitation. The 31-day smoothing approach is further justified by the work of Hirons et al. (2018), who demonstrated that an AGCM with high-frequency SSTs overestimated precipitation extremes, relative to satellite-derived responses.

Tracking of monsoon LPS is carried out using TRACK software (Hodges 1994) with additional criteria specifically for Indian monsoon LPS following the methodology described in Levine and Martin (2018). The tracking is carried out by first filtering the vorticity data to a common T42 resolution in all cases, therefore there is no resolution dependence in the tracking method (Hodges 1994; Levine and Martin 2018).

ERA5 (ERA5; Copernicus Climate Change Service (C3S) (2017)) re-analysis data of 850hPa winds on a 6-hourly time-scale and at $0.25^\circ \times 0.25^\circ$ horizontal resolution are used for diagnosing monsoon LPS in observations and monthly mean ERA5 data for atmospheric winds, temperature and relative humidity are used for model comparison. Observational data for precipitation are taken from the APHRODITE data-set (Yatagai et al. 2009), as this has sufficiently high temporal (daily) and spatial (0.25°) resolution, although does not include coverage over the ocean, and currently only reaches up to 2007. Therefore, the observational data of the LPS tracks is analysed for the 1983-2007 period, which is still sufficient to compute a climatological average of monsoon LPS rainfall for comparison with the model data. GPCP monthly mean precipitation is used for evaluating the wider area mean conditions in the simulations (Adler et al 2003).

3 Results

3.1 Reanalysis and observations

We start by discussing the LPS detected in the ERA5 re-analysis, before moving to a comparison with the model simulations. Properties of these tracks combined with APHRODITE rainfall data are shown in Fig. 1. The track density in this figure is calculated as

$$\rho_{i,j} = \left[\sum_t \delta_{i,j,t} \right] / \left[\sum_{i,j} \sum_t \delta_{i,j,t} \right] \quad (1)$$

where $\delta = 1$ if a track is present at (i, j, t) or $\delta = 0$ otherwise, for all 6-hourly time-steps during LPS lifetimes. The coordinates i, j and t represent longitude, latitude and time respectively. Genesis density is calculated in a similar fashion:

$$\phi_{i,j} = \left[\sum_{\text{LPS}} \delta_{i,j,t_0} \right] / \left[\sum_{i,j} \sum_{\text{LPS}} \delta_{i,j,t_0} \right] \quad (2)$$

where t_0 is the first time-step for each LPS.

There are 212 LPS diagnosed in ERA5 in the 1983-2007 period during June to September, which is equivalent to almost 8.5 systems per monsoon season. The

Table 1 List of simulations. *ATM* represents an atmosphere-only simulation. *GL* represents the MetUM-GOML2 globally coupled simulation. Regionally coupled MetUM-GOML2 simulations are represented by *IO* (Indian Ocean), *PO* (Pacific Ocean), *AO* (Atlantic Ocean), *IO_PO* (Indian and Pacific Oceans), etc. *GC2* represents the fully coupled MetUM-GC2 configuration simulation. Sub-scripts show the horizontal resolution in km (either 200km or 90km). The value in brackets for atmosphere-only simulations indicates the SST used (*[obs]* for observational SST, *[GL]* for MetUM-GOML2 globally coupled SST, *[IO]* for MetUM-GOML2 Indian Ocean coupled SST, etc.)

Description	Atmosphere-Ocean Coupling	(MetUM) Resolution	Years
<i>ATM</i> ₂₀₀ <i>[obs]</i>	None - AMIP run (obs SST)	200km (N96)	1983-2010
<i>ATM</i> ₉₀ <i>[obs]</i>	None - AMIP run (obs SST)	90km (N216)	1983-2010
<i>GC2</i> ₂₀₀	Fully 3D coupled MetUM	200km (N96)	28 years (present day control run)
<i>GC2</i> ₉₀	Fully 3D coupled MetUM	90km (N216)	28 years (present day control run)
<i>GL</i> ₂₀₀	GOML2 Global (constrained to obs)	200km (N96)	28 years
<i>AO_PO</i> ₂₀₀	GOML2 Global, EXCEPT Indian Ocean	200km (N96)	28 years
<i>IO</i> ₂₀₀	GOML2 Indian Ocean only	200km (N96)	28 years
<i>PO</i> ₂₀₀	GOML2 Pacific Ocean only	200km (N96)	28 years
<i>IO_PO</i> ₂₀₀	GOML2 Indian and Pacific Oceans	200km (N96)	28 years
<i>ATM</i> ₂₀₀ <i>[IO]</i>	None - SSTs from <i>IO</i> ₂₀₀ (31-day smoothed)	200km (N96)	28 years
<i>ATM</i> ₂₀₀ <i>[GL]</i>	None - SSTs from <i>GL</i> ₂₀₀ (31-day smoothed)	200km (N96)	28 years
<i>GL</i> ₉₀	GOML2 Global (constrained to obs)	90km (N216)	28 years
<i>AO_PO</i> ₉₀	GOML2 Global EXCEPT Indian Ocean	90km (N216)	28 years
<i>IO</i> ₉₀	GOML2 Indian Ocean only	90km (N216)	28 years
<i>PO</i> ₉₀	GOML2 Pacific Ocean only	90km (N216)	28 years
<i>IO_PO</i> ₉₀	GOML2 Indian and Pacific Oceans	90km (N216)	28 years
<i>ATM</i> ₉₀ <i>[IO]</i>	None - SSTs from <i>IO</i> ₉₀ (31-day smoothed)	90km (N216)	28 years
<i>ATM</i> ₉₀ <i>[GL]</i>	None - SSTs from <i>GL</i> ₉₀ (31-day smoothed)	90km (N216)	28 years
<i>ERA5/APHRO</i>	atm U, V, T, RH from re-analysis / obs land-only precip	0.25° / 0.25°	1983-2007

368 systems mainly originate in the northern Bay of Ben-
369 gal, with further systems developing within the mon-
370 soon trough over north eastern India. During the early
371 monsoon a small number of cyclonic systems develop
372 over the eastern Arabian Sea. The combined effects of
373 the LPS contribute a substantial amount of rainfall to
374 the north-eastern and northern areas of India.

375 3.2 Standard MetUM simulations and 376 MetUM-GOML2 SST biases

377 In this section results are presented from standard AMIP-
378 style atmosphere only simulations forced with observed
379 SST (*ATM**[obs]*) and fully coupled atmosphere-ocean
380 simulations (*GC2*). The *GC2* simulations have substan-
381 tial SST biases, both local and remote to the Indian
382 Ocean sector (eg. Fig. 2a in Wainwright et al. 2019).
383 Effects of local Indian Ocean SST biases on the Indian
384 monsoon have been shown for a previous version of the
385 MetUM in Levine and Turner (2012), with northern
386 Indian Ocean and equatorial Indian Ocean cold SST
387 biases having counteracting effects. However, the cold
388 SST bias over the Arabian Sea dominated in that par-
389 ticular version of the model, resulting in weakened mon-
390 soon winds and rainfall. This pattern of cold SST biases,
391 although smaller in magnitude, is still persistent in the
392 *GC2* configuration used in this study, but it appears
393 that there is less influence from the cold bias over the
394 Arabian Sea.

395 The SST biases in the MetUM-GOML2 simulations
396 discussed in this study are shown in Fig. 2. This shows
397 that there is still a cold SST bias present over the

equatorial Indian Ocean at both horizontal resolutions,
which may influence the Indian monsoon and LPS. A
direct impact of this could be to strengthen the mon-
soon circulation, as expected from experiments using
a previous configuration of the MetUM (Levine and
Turner, 2012). However, differences in the magnitude
or area of the SST bias may result in other impacts,
while other models may behave differently (Bollasina
and Nigam 2009; Prodhomme et al. 2014). There is also
the potential for remote SST biases over the Atlantic
or Pacific Oceans to influence the monsoon indirectly
through atmospheric teleconnections.

The cold SST biases in the Indian Ocean are pri-
marily the result of errors in atmospheric wind-stress
forcing of the ocean, which cannot be eliminated us-
ing the temperature and salinity corrections. Excessive
wind-driven oceanic vertical mixing cools SST, but also
means that the temperature corrections applied are too
readily mixed. The temperature corrections attempt to
restratify the ocean and shoal the mixed layer – by
warming near the surface and cooling at depth – but
these corrections are ineffective as they are mixed across
the (deeper) mixed layer by the atmospheric wind forc-
ing. The strength of the cold SST biases does not de-
pend strongly on the nudging timescale used in the ini-
tial MetUM-GOML2 relaxation simulation. Shortening
the nudging timescale would strengthen the tempera-
ture corrections, but retain their vertical profile – warm-
ing near the surface and cooling at depth – resulting
in nearly zero net change to oceanic heat content and
hence similar biases in SST and mixed-layer depth. For
further details, see Hirons et al. (2015).

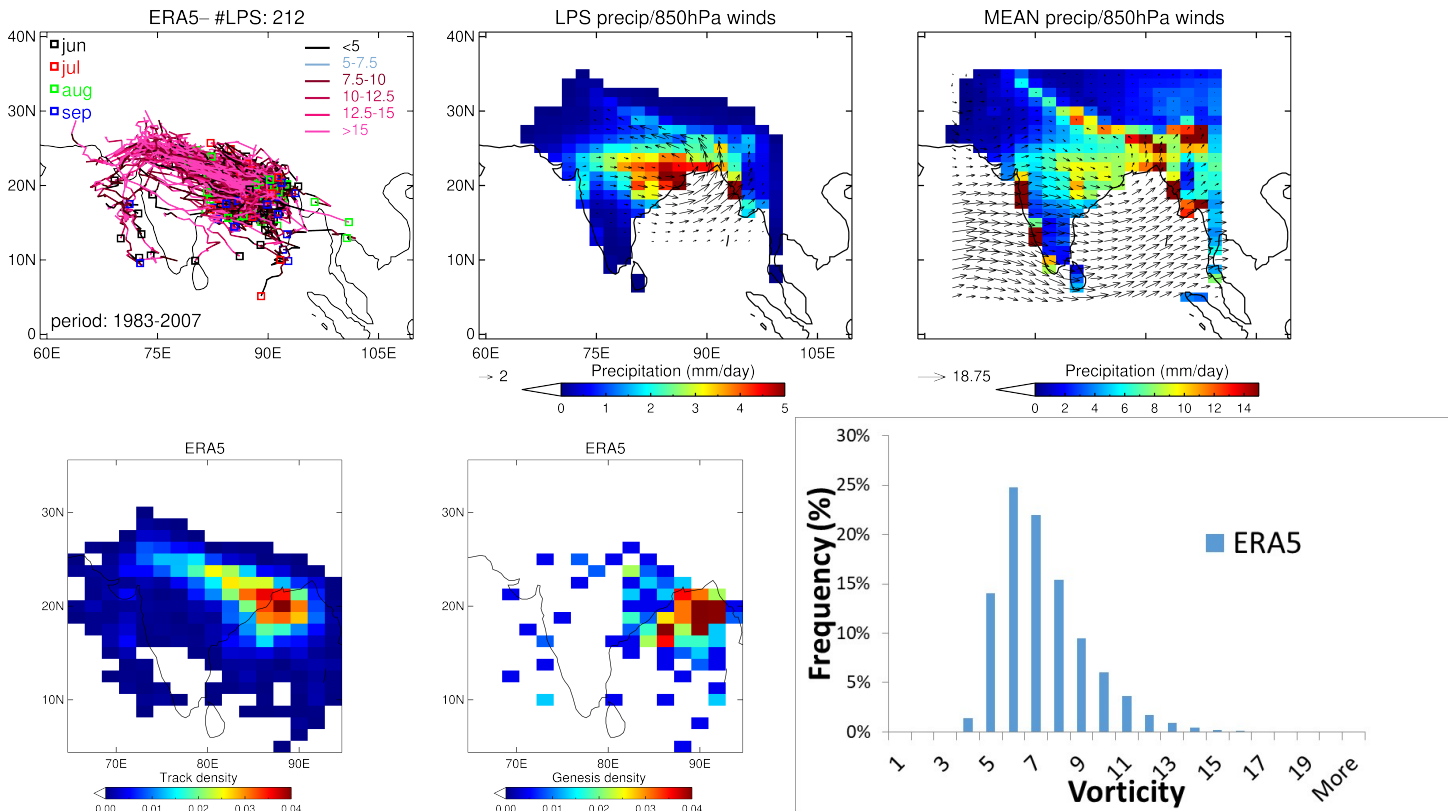


Fig. 1 Monsoon LPS diagnosed in ERA5 re-analysis for 1983-2007 with APHRODITE land precipitation statistics. On the top row: the *first panel on left hand-side* shows LPS trajectories with the total number of LPS in title. The coloured squares indicate the starting point and month of each track. The colour of the trajectories indicates the strength in terms of relative vorticity ($10^{-5} s^{-1}$ at native resolution). The *second panel from left* shows LPS contribution to JJAS seasonal precipitation (mm/day) and 850 hPa winds (m/s, black vectors). The *third panel from left* shows Jun-Sept seasonal mean precipitation (mm/day) and 850 hPa winds (m/s, black vectors). All data is plotted on a 200km (N96; $1.875^\circ \times 1.25^\circ$) grid. Bottom row shows TRACK DENSITY, GENESIS DENSITY and a HISTOGRAM of LPS intensity. The intensity is shown in terms of relative vorticity (in units of $10^{-5} s^{-1}$) filtered to T42 resolution (as used in tracking) at the centre of the system at the 850hPa level, and includes all 6-hourly time-steps during LPS lifetime. These ERA5 figures have been generated using Copernicus Climate Change Service Information 2020.

430 The results of LPS analysis for $ATM_{90}[obs]$, GC_{90} ,
 431 GL_{90} and $ATM_{90}[GL]$ are shown in Fig. 3. An equiv-
 432 alent comparison for the 200km (N96) simulations has
 433 qualitatively similar results and is not shown. The Me-
 434 tUM simulations have substantially less LPS activity
 435 than ERA5, while activity is far more spatially limited
 436 to the Bay of Bengal, with only a few systems trav-
 437 elling westwards across India in the monsoon trough.
 438 This lack of LPS in global simulations, and the inabil-
 439 ity to propagate over Indian land, is a typical feature
 440 of MetUM climate configurations (Levine and Martin,
 441 2018). The $ATM_{90}[obs]$ has only 76 LPS, or 2.7 LPS
 442 per season, which is approximately 32% of the num-
 443 ber in ERA5. This coincides with the consistently weak
 444 monsoon in the MetUM (e.g. Johnson et al. 2016). The
 445 fully coupled GC_{290} simulation has a few more sys-
 446 tems and associated LPS rainfall, which coincides with
 447 stronger westerly low-level winds across the Arabian

448 Sea, India and the Bay of Bengal. There is also more
 449 rainfall across this band, although not much over In-
 450 dian land. Differences between GC_{90} and $ATM_{90}[obs]$
 451 could be due to many factors, including direct effects
 452 of coupling on LPS, local or remote effects of coupling
 453 on the monsoon circulation, direct effects of local SST
 454 biases on LPS, or local or remote effects of SST biases
 455 on the monsoon circulation.

456 The MetUM-GOML2 mixed-layer ocean coupled sim-
 457 ulation GL_{90} shows quite similar changes to GC_{290} ,
 458 though there are now substantially more systems (4.4
 459 on average per season, or approximately half of the
 460 number in ERA5). This coincides with more LPS rain-
 461 fall, which now also starts to show some impact on mean
 462 rainfall over NE India. There could be numerous rea-
 463 sons for the differences with GC_{290} , for example a local
 464 impact could be the strengthening of the monsoon cir-
 465 culation due to a change in the balance of northern

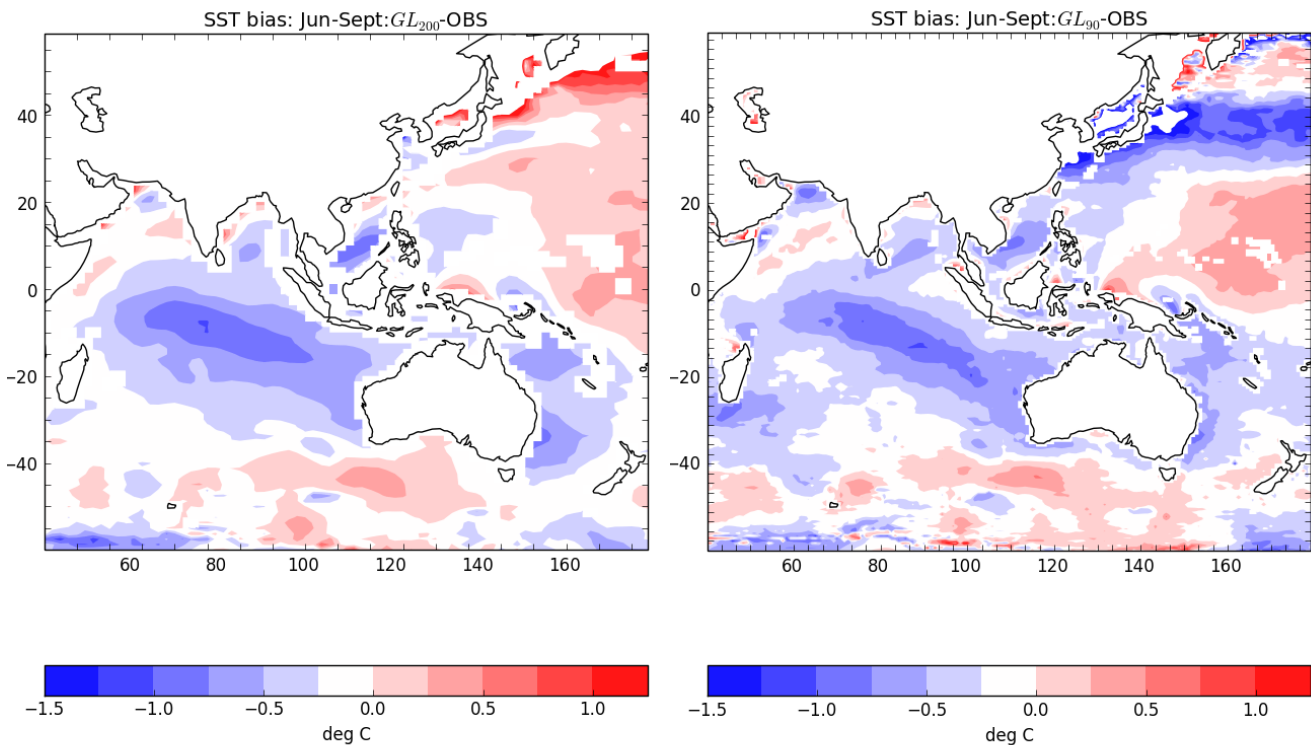


Fig. 2 Climatological JJAS SST biases for GL_{200} and GL_{90} compared to Smith and Murphy (2007) observations.

466 and equatorial Indian Ocean SST biases, thereby pro- 466
 467 viding more favourable conditions for LPS formation. 467
 468 The comparison with $ATM_{90}[GL]$ allows some more 468
 469 definite conclusions on the effects of SST biases. The 469
 470 $ATM_{90}[GL]$ simulation is very close to GL_{90} in terms of 470
 471 differences with the $ATM_{90}[obs]$ standard AMIP-type 471
 472 simulation. This suggests that coupling is not a major 472
 473 influence in the changes seen in the latter three rows 473
 474 of 3 with respect to $ATM_{90}[obs]$, which therefore are 474
 475 quite likely the result of SST biases. It should be noted 475
 476 that the AMIP-type runs also contain variability due 476
 477 to ENSO and IOD events in the SST forcing, while the 477
 478 atmosphere-only runs forced with the coupled SST do 478
 479 not contain such variability due to the smoothing ap- 479
 480 plied. This is likely to affect the interannual variability 480
 481 in LPS and may also affect the mean number of LPS 481
 482 due to non-linear effects. 482

483 It is also worth noting that Peatman and Klingaman 483
 484 (2018) has investigated the role of intra-seasonal 484
 485 variability (ISV), interannual variability (IAV) and SST 485
 486 biases in differences in the mean state atmosphere pre- 486
 487 sented due to coupling in different basins, and it is con- 487
 488 cluded that these are mainly attributable to SST biases. 488
 489 The $GL - AO_{PO}$ differences (Peatman and Klingaman 489
 490 (2018), Figs. 3a,c) then give an approximation of the ef- 490
 491 fects of Indian Ocean SST biases, which are to cause a

492 relative reduction of precipitation over the equatorial 492
 493 Indian Ocean and increase to the north of this, while 493
 494 there are no significant changes over Indian land. This 494
 495 is accompanied by strengthening of the low-level mon- 495
 496 soon jet starting from the Bay of Bengal and extending 496
 497 through the South China Sea into the W Pacific. While 497
 498 the latter is consistent with the effects seen in this study 498
 499 (Fig. 3, note different scales) in $ATM[GL] - ATM[obs]$, 499
 500 the biases in the mean state precipitation in this case 500
 501 are more widespread and larger than the aforemen- 501
 502 tioned $GL - AO_{PO}$ changes in Peatman and Klingaman 502
 503 (2018), which must then be explained by effects of 503
 504 missing IAV and/or ISV in the $ATM[GL]$ experiments 504
 505 and possibly the role of any of these processes feeding 505
 506 back on each other. 506

507 The precise attribution of changes to the monsoon 507
 508 circulation and LPS to localised SST biases and their 508
 509 mechanisms is beyond the scope of this study. How- 509
 510 ever, while the atmospheric monsoon base state may 510
 511 be slightly different from the standard fully coupled 511
 512 and AMIP-style MetUM simulations, the isolated com- 512
 513 parison of MetUM-GOML2 mixed-layer ocean coupled 513
 514 simulations and their equivalent atmosphere-only sim- 514
 515 ulations (forced with GOML2 SST) does provide for 515
 516 a somewhat idealised decomposition into effects from 516
 517 coupling and from resolution. 517

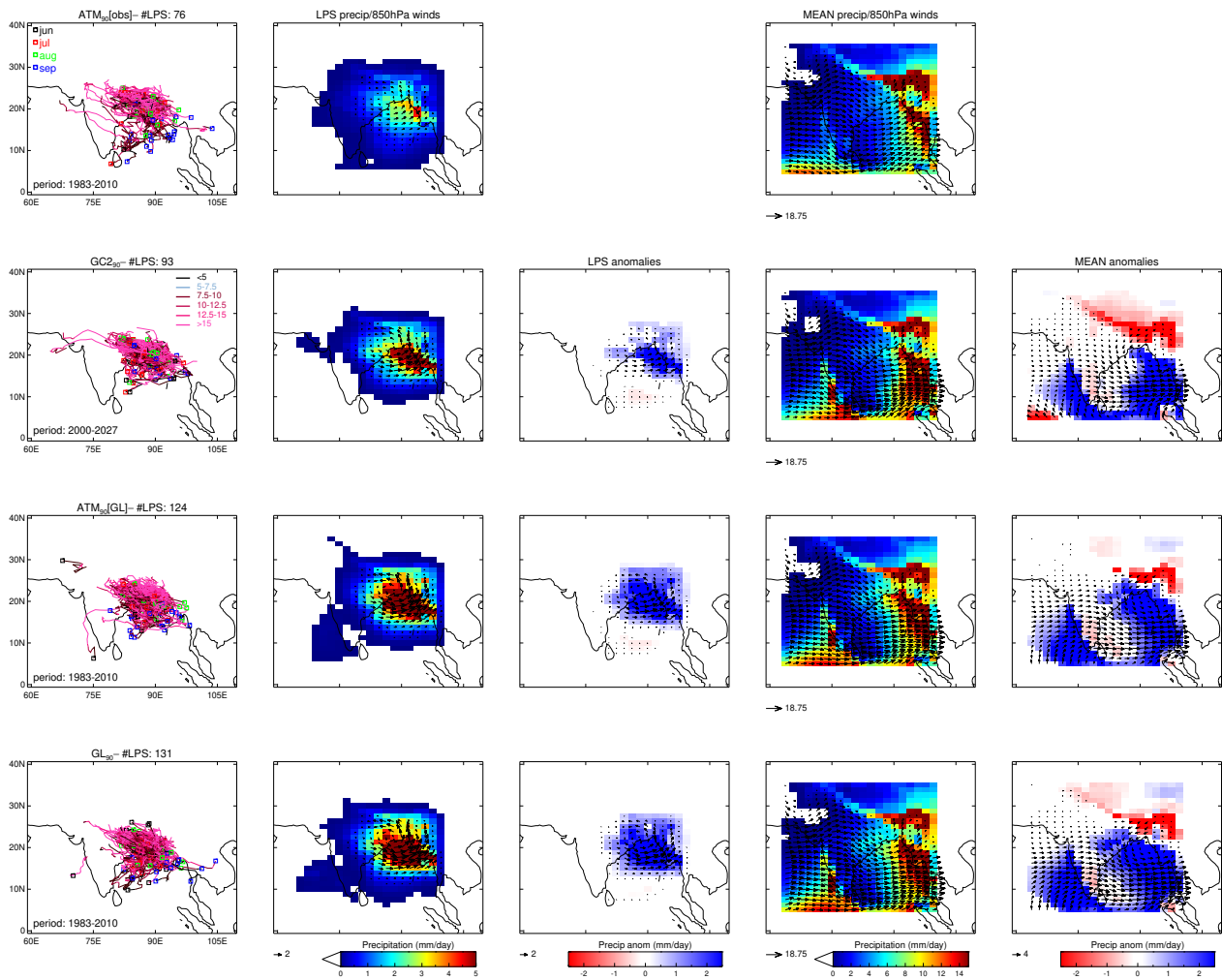


Fig. 3 Monsoon LPS diagnosed in 90km (N216) experiments for 1983-2010 period. Top row shows the $ATM_{90}[\text{obs}]$ experiment, with subsequent rows showing results for $GC2_{90}$, GL_{90} and $ATM_{90}[GL]$. Differences are all in comparison to $ATM_{90}[\text{obs}]$. The **first panel on left hand-side** shows LPS trajectories with the total number of LPS in title. The coloured squares indicate the starting point and month of each track. The colour of the trajectories indicates the strength in terms of relative vorticity ($10^{-5} s^{-1}$ at native resolution). The **second panel from left** shows LPS contribution to JJAS seasonal mean precipitation (mm/day) and 850 hPa winds (m/s, black vectors). The **third panel from left** shows difference in LPS precipitation and 850hPa wind contributions with respect to top row experiment. The **fourth panel from left** shows Jun-Sept seasonal mean precipitation (mm/day) and 850 hPa winds (m/s, black vectors). The **fifth panel from left** shows difference in Jun-Sept seasonal mean and 850hPa wind contributions with respect to top row experiment. Data are plotted on a common 200km (N96; $1.875^\circ \times 1.25^\circ$) grid. Only significant differences and vectors at 90% level using a student t-test are shown. Values exceeding the colour scale maxima are capped at the relevant maximum colour value.

518 3.3 Role of air-sea coupling

519 In order to isolate the effects of the air-sea coupling,
 520 each coupled simulation is compared to the equivalent
 521 atmosphere-only simulation forced with (31-day smoothed)
 522 SSTs from the coupled simulation. In this way, for ex-
 523 ample, the GL_{200} simulation should be compared to
 524 $ATM_{200}[GL]$. However, we also compare against the
 525 atmosphere-only simulation forced with observed SSTs

in order to interpret the results from the regionally-
 coupled simulations.

3.3.1 Global coupling

The number of monsoon LPS in GL_{200} (81, equivalent
 to 2.9 LPS per JJAS season on average) and $ATM_{200}[GL]$
 (75, equivalent to 2.7 LPS per season on average) is
 similar, though there is an eastward shift visible in the
 location of the LPS trajectories and the resulting rain-

526

527

528

529

530

531

532

533

fall in GL_{200} (Fig. 4). In the coupled simulation the LPS appear to produce marginally less rainfall, while the trajectories and rainfall are somewhat more constrained over the Bay of Bengal and do not move as far westwards across northern India as in observations. This reduced rainfall over the monsoon trough helps explain the differences between these simulations in the mean seasonal JJAS rainfall, the main feature of which is weaker rainfall over much of India and the BoB in GL_{200} . The comparison of GL_{200} with $ATM_{200}[obs]$ in Fig. 4 further highlights that the combined effect of differences in interannual SST variability and SST biases in GL_{200} results in a strengthening of the seasonal mean monsoon and increased LPS activity in GL_{200} . This is an important consideration when interpreting the locally coupled simulations in later sections.

The percentage of seasonal rainfall change due to changes in LPS is shown in Fig. 5. This is calculated as

$$\Delta = 100\% \times \left[\frac{Pr_{LPS}(GL) - Pr_{LPS}(ATM[GL])}{Pr(GL) - Pr(ATM[GL])} \right], \quad (3)$$

where Pr is mean JJAS precipitation and Pr_{LPS} is LPS rainfall over the same period.

This highlights that the changes over India and the BoB are to a large degree attributable to LPS. The damping effect of air-sea coupling on LPS rainfall over the BoB is consistent with the localised effect of air-sea coupling on tropical rainfall seen in previous studies (eg. Hirons et al. 2018).

Both 200km (N96) MetUM simulations have substantially fewer LPS and less LPS rainfall than diagnosed in ERA5 and APHRODITE (cf. Fig. 1). The trajectories in the re-analysis also reach substantially further westwards across northern India within the monsoon trough. This lack of LPS in global simulations, and the inability to propagate over Indian land, is a typical feature of MetUM climate configurations (Levine and Martin, 2018).

These common biases in LPS representation with respect to observations/reanalysis are likely the result of the overall weak monsoon circulation in this configuration as also seen in AMIP-style simulations in previous configurations of the MetUM (eg. Johnson et al. 2016). The relatively weak Somali Jet, the lack of rainfall over India, the excessive rainfall over the equatorial Indian Ocean and Himalayan foothills are all part of this, and make for unfavourable conditions for LPS formation and westward propagation over the relatively dry Indian land. It has been shown in Levine and Martin (2018) using regional climate model simulations that substantial improvements are seen when the inflow conditions into the Indian sector are corrected, including the probable effect of pre-cursor disturbances from the W Pacific.

3.3.2 Coupling in individual basins

In this section the effect of coupling in individual basins is examined in the 200km (N96) simulations (Figure 6). Among these simulations, the global coupling experiment produces the most LPS, which appear to play a role in differences in seasonal-mean precipitation over Indian land. On the other hand, the experiments without coupling over the Indian Ocean produce the fewest LPS and least LPS rainfall, suggesting local coupling is important for Indian monsoon LPS formation.

The effects of coupling will be examined two ways, using two different reference states. The first uses GL_{200} as the reference simulation. In this way we examine the contribution to the overall effect of global coupling from the following four areas:

1. **Coupling INSIDE Indian Ocean only:** $GL_{200} - AO_PO_{200}$ (Fig. 6, second row),
2. **Coupling OUTSIDE Indian Ocean:** $GL_{200} - IO_{200}$ (Fig. 6, third row),
3. **Coupling OUTSIDE Pacific Ocean:** $GL_{200} - PO_{200}$ (Fig. 6, fourth row),
4. **Coupling OUTSIDE Indian and Pacific Oceans:** $GL_{200} - IO_PO_{200}$ (Fig. 6, fifth row).

The first of these ($GL_{200} - AO_PO_{200}$) indicates the effect of adding Indian Ocean coupling in comparison to a base state where (i) there is already air-sea coupling in the Atlantic and Pacific Oceans; (ii) there are MetUM-GOML2 mean SST biases in all three basins (Indian, Pacific and Atlantic Oceans); and (iii) there are no coupled modes of variability like ENSO or the IOD.

In general, the contribution from coupling over the Indian Ocean ($GL_{200} - AO_PO_{200}$) to the effects of global coupling on Indian monsoon LPS rainfall is similar, and of the same sign, to that from coupling outside the Indian Ocean ($GL_{200} - IO_{200}$). This suggests that both coupling within and outside the Indian Ocean have a positive effect of similar magnitude, which is particularly evident in monsoon LPS rainfall. In terms of JJAS mean rainfall, in addition to the effects over India and the BoB from the monsoon LPS, there is a more widespread positive effect from coupling within the Indian Ocean on rainfall over the Arabian Sea, BoB and equatorial Indian Ocean.

Of the other areas shown, there is a neutral effect from coupling outside the Indian and Pacific Oceans ($GL_{200} - IO_PO_{200}$). This suggests that the positive effects from coupling outside the Indian Ocean ($GL_{200} - IO_{200}$), as discussed earlier, are primarily due to effects of coupling over the Pacific Ocean. Furthermore, the effects of coupling outside the Pacific Ocean (GL_{200}

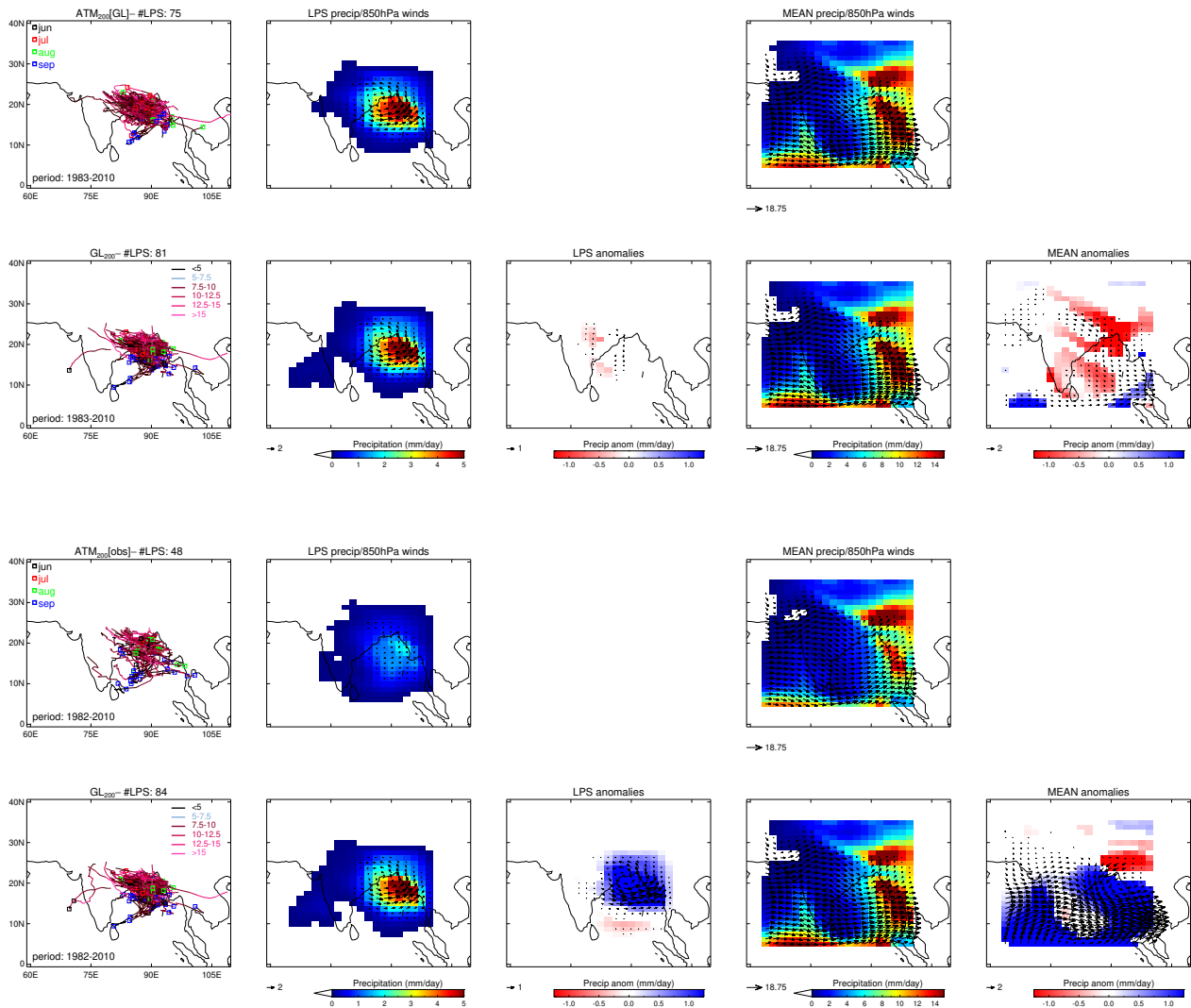


Fig. 4 Monsoon LPS diagnosed in 200km (N96) experiments for 1983-2010 period. Top row shows the $ATM_{200}[GL]$ experiment, second row shows the GL_{200} experiment, with differences displayed as $[GL_{200} - ATM_{200}[GL]]$. The same comparison is shown for GL_{200} with $ATM_{200}[obs]$ in the third and fourth rows. The **first panel on left hand-side** shows LPS trajectories with the total number of LPS in title. The coloured squares indicate the starting point and month of each track. The colour of the trajectories indicates the strength in terms of relative vorticity ($10^{-5} s^{-1}$ at native resolution). The **second panel from left** shows LPS contribution to JJAS seasonal mean precipitation (mm/day) and 850 hPa winds (m/s, black vectors). The **third panel from left** shows difference in LPS precipitation and 850hPa wind contributions with respect to top row experiment. The **fourth panel from left** shows Jun-Sept seasonal mean precipitation (mm/day) and 850 hPa winds (m/s, black vectors). The **fifth panel from left** shows difference in Jun-Sept seasonal mean and 850hPa wind contributions with respect to top row experiment. All data in panels two, three, four and five are plotted on a common 200km (N96; $1.875^\circ \times 1.25^\circ$) grid. Only significant differences and vectors at 90% level using a student t-test are shown. Values exceeding the colour scale maxima are capped at the relevant maximum colour value.

637 - PO_{200}) are very similar to the effects of coupling out- 644
 638 side the Indian Ocean ($GL_{200} - IO_{200}$). 645

639 However, it is important to note that these (ap- 646
 640 parent positive) effects are of the opposite sign to the 647
 641 $GL_{200} - ATM_{200}[GL]$ comparison, which suggested a 648
 642 neutral-negative effect of global coupling when refer- 649
 643 enced to the equivalent atmosphere-only simulation. This 650

discrepancy can occur due to various reasons. Firstly, 644
 the uncoupled regions in IO_{200} , PO_{200} , etc. are pre- 645
 scribed with climatological monthly-varying observed 646
 SST, which does not contain interannual SST variabil- 647
 ity that is present in the globally coupled simulation 648
 and the atmosphere-only simulation forced with SST 649
 from the globally coupled simulation. Secondly, the re- 650

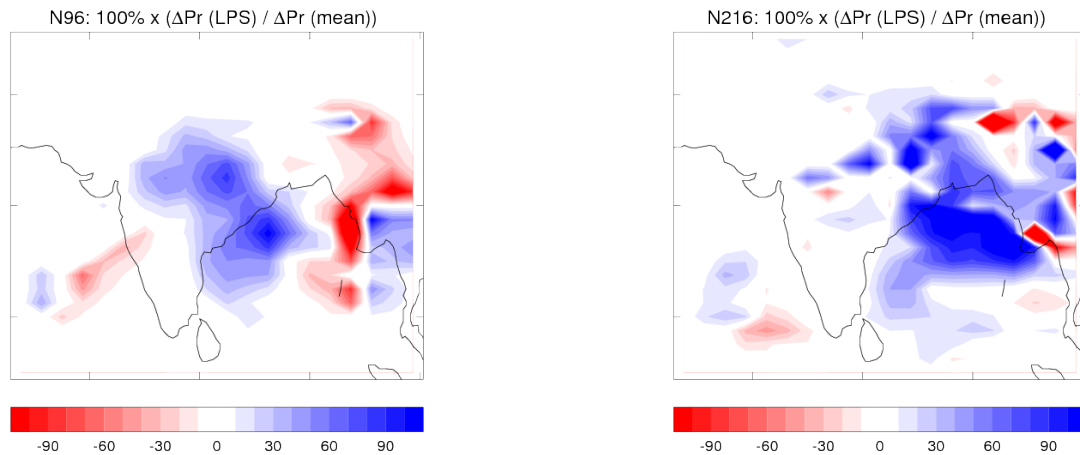


Fig. 5 Percentage of seasonal change in rainfall due to LPS in N96 (200km, on left) and N216 (90km, on right) global coupling experiments. Calculated as in eq. 3. Grid-boxes where mean precipitation change $|Pr(GL) - Pr(ATM[GL])| < 0.1$ mm/day have been masked out (set to zero). Note that values can exceed $\pm 100\%$ due to compounding/compensating changes in mean rainfall from sources other than LPS.

651 maining SST biases in the globally coupled simulation
 652 are not present in the uncoupled regions of the re-
 653 gionally coupled simulations. The $GL_{200} - ATM_{200}[obs]$
 654 comparison in Fig. 4, which shows a strengthening of
 655 the monsoon and LPS in GL_{200} due to differences in in-
 656 terannual SST variability and SST bias, suggests that
 657 the positive signals found in the previous comparison of
 658 the locally coupled simulations may be (at least partly)
 659 for the same reason. Thirdly, there may be interaction
 660 between the effects of coupling in different basins. How-
 661 ever, it should be emphasized that the first two factors
 662 do not affect the $GL_{200} - ATM_{200}[GL]$ comparison.

663 The second comparison uses $ATM_{200}[obs]$ as the
 664 reference simulation in order to examine the effect of
 665 coupling in each of the different regions versus no cou-
 666 pling at all. In this case the mean SST in the uncoupled
 667 regions (climatological monthly-varying observed SST
 668 from Met Office ocean analyses) remains relatively con-
 669 sistent in all the simulations with the observed SST
 670 from Reynolds et al. (2007) in the atmosphere-only
 671 AMIP-type run ($ATM_{200}[obs]$). Global coupling ($GL_{200} -$
 672 $ATM_{200}[obs]$) has already been shown in this manner in
 673 Fig. 4.

674 5. Coupling INSIDE Atlantic and Pacific Oceans:

675 $AO_{PO_{200}} - ATM_{200}[obs]$ (Fig. 7, second row),

676 6. Coupling INSIDE Indian Ocean only: $IO_{200} -$
 677 $ATM_{200}[obs]$ (Fig. 7, third row),

678 7. Coupling INSIDE Pacific Ocean only: PO_{200}
 679 $- ATM_{200}[obs]$ (Fig. 7, fourth row),

680 8. Coupling INSIDE Indian and Pacific Oceans:
 681 $IO_{PO_{200}} - ATM_{200}[obs]$ (Fig. 7, fifth row).

682 For example, the $IO_{200} - ATM_{200}[obs]$ comparison
 683 indicates the effect of adding Indian Ocean coupling

684 compared to a base state where (i) the Atlantic and
 685 Pacific Oceans are not coupled; (ii) the mean SST in the
 686 Atlantic and Pacific Oceans is similar to observed; and
 687 (iii) there are coupled modes of variability like ENSO
 688 present.

689 The results suggest that the combined Indian and
 690 Pacific Ocean coupling $IO_{PO_{200}} - ATM_{200}[obs]$ has
 691 the largest effect, similar but slightly weaker than the
 692 equivalent global coupling response $GL_{200} - ATM_{200}[obs]$
 693 (Fig. 4), while the biggest single influence comes from
 694 Indian Ocean coupling. Differences between the two
 695 comparisons of coupling inside the Indian Ocean (GL_{200}
 696 $- AO_{PO_{200}}$ and $IO_{200} - ATM_{200}[obs]$) are relatively
 697 small, and may reflect the effect of differences in in-
 698 terannual SST variability between the reference simu-
 699 lations.

700 In summary, while there are the caveats with respect
 701 to differences in SST biases and variability, both com-
 702 parisons point to the largest sensitivity coming from
 703 air-sea coupling in the Indian Ocean and Pacific Ocean
 704 basins.

705 3.4 Role of horizontal resolution

706 3.4.1 Impact of increase in horizontal resolution

707 The ATM_{90} and GL_{90} higher resolution simulations are
 708 compared to the observations in Fig. 8. The main fea-
 709 ture is that the increase in resolution from 200km (N96)
 710 to 90km (N216) results in substantially more LPS ac-
 711 tivity and increased LPS rainfall (cf. Fig. 4). The num-
 712 ber of monsoon LPS in GL_{90} is 131 (equivalent to 4.7
 713 LPS per JJAS season on average), while $ATM_{90}[GL]$

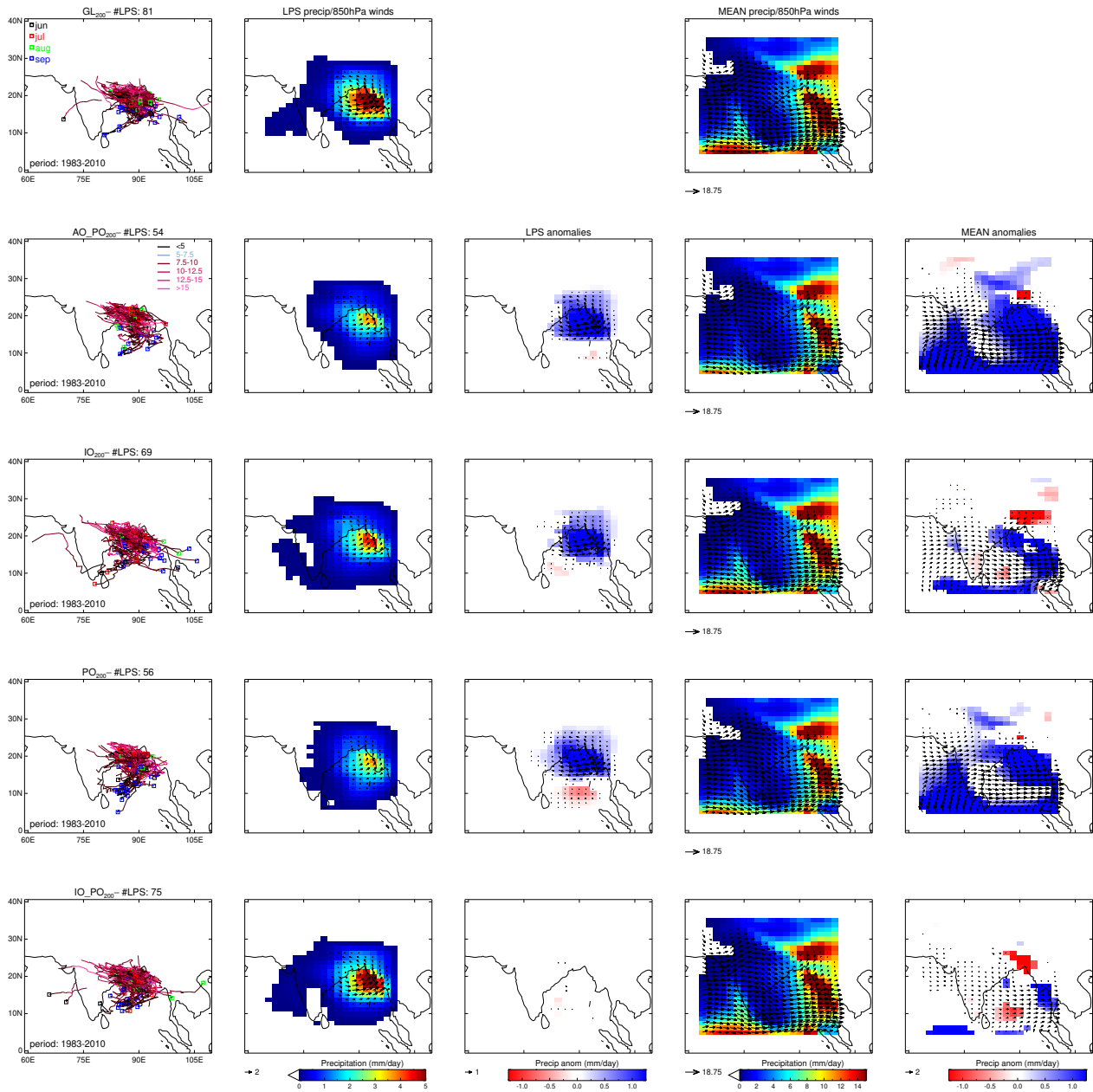


Fig. 6 Coupling sensitivity of 200km (N96) simulations for 1983-2010 period. Top row shows the Global Coupling (obs) experiment, while subsequent rows show the results for regional coupling and differences displayed as $[GL_{200} - AO_{PO_{200}}]$ (coupling INSIDE Indian Ocean), $[GL_{200} - IO_{200}]$ (coupling OUTSIDE Indian Ocean), $[GL_{200} - PO_{200}]$ (coupling OUTSIDE Pacific Ocean), $[GL_{200} - IO_{PO_{200}}]$ (coupling OUTSIDE Indian and Pacific Oceans). The layout of the plots is as described in Fig. 4.

714 has a similar number (124, equivalent to 4.4 LPS per
 715 season on average). These are closer to the observed
 716 number (6.8 per JJAS season) than the lower resolu-
 717 tion 200km (N96) simulations. As stated previously, the
 718 results from the LPS tracking are independent of resolu-
 719 tion, therefore the improvements at higher resolution
 720 are due to the model capturing the LPS more accu-

rately. In both the atmosphere-only and coupled 90km
 (N216) simulations the systems form over a larger area
 of the BoB than is the case for the 200km (N96) sim-
 ulations, which is somewhat more in line with obser-
 vations. The LPS are also somewhat more realistic as
 they travel further north-westwards across the BoB and
 northern India at higher resolution.

721
 722
 723
 724
 725
 726
 727

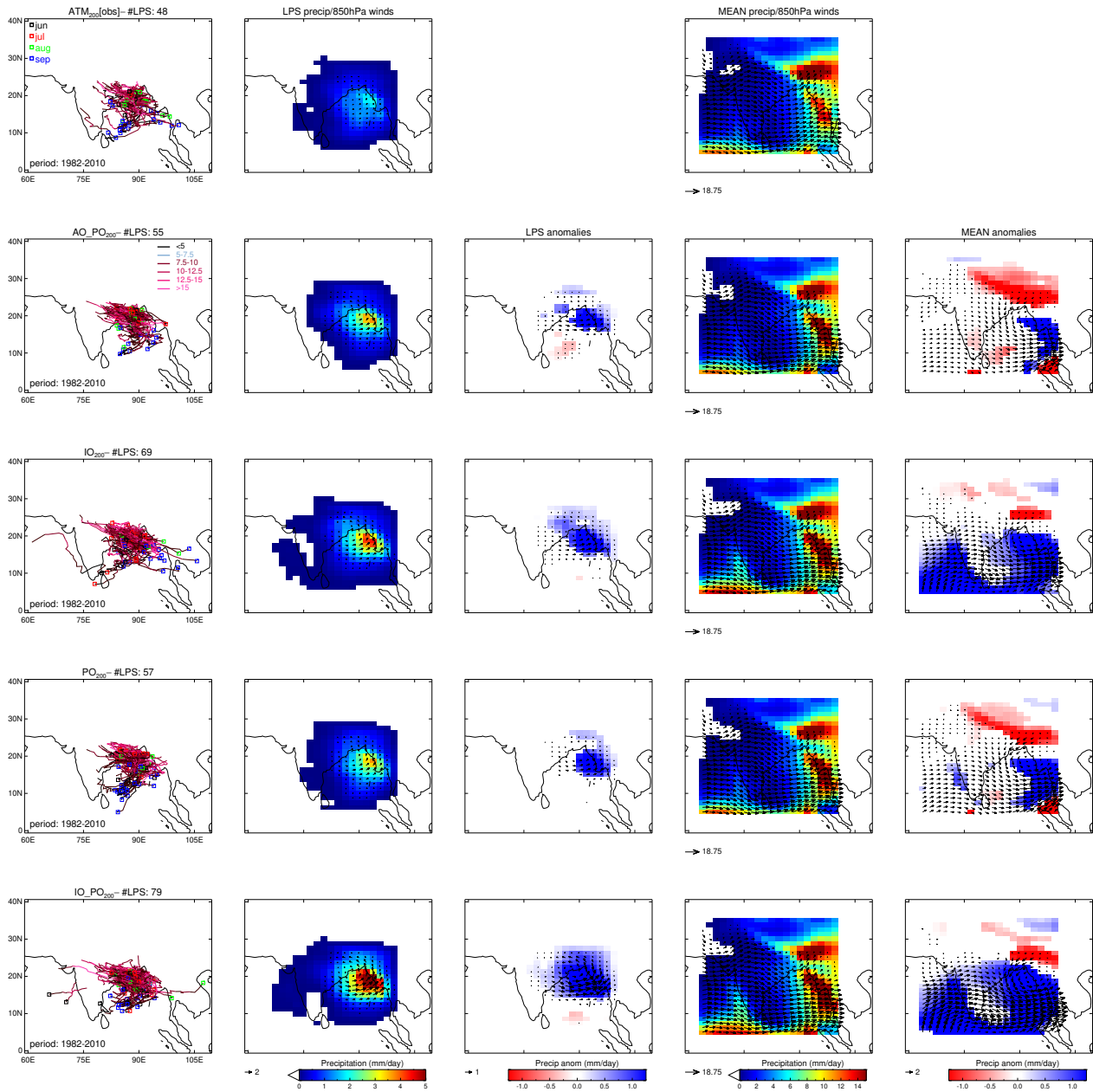


Fig. 7 Coupling sensitivity of 200km (N96) simulations for 1983-2010 period. Top row shows the Atmosphere-only experiment, while subsequent rows show the results for regional coupling and differences displayed in the following form $[IO200] - ATM_{200}[obs]$. The layout of the plots is as described in Fig. 4.

728 There are several factors which likely combine to
 729 result in the improvements with increased horizontal
 730 resolution. Firstly, better resolving the structure of the
 731 LPS. Using the same MetUM configuration (GA6) using
 732 initialised NWP simulations of monsoon depressions,
 733 Hunt and Turner (2017) found the greatest improve-
 734 ments with changes in horizontal resolution when
 735 moving from N96 (denoted in this paper as 200km)
 736 to N216 (denoted in this paper as 90km), with little

improvement beyond that. This indicates that there
 should be an improvement in resolving the structure
 of the LPS in our higher resolution simulations.

The second factor is improvement to the wider re-
 gion circulation. Levine and Martin (2018) and Karma-
 charya et al (2015, 2016), using an older configura-
 tion of the MetUM (GA3, without the ENDGAME dynam-
 ical core improvements in GA6), found that horizon-
 tal resolution (in this case from 50km to 12km) plays

737
 738
 739
 740
 741
 742
 743
 744
 745

a smaller role than improving the wider region circulation, in particular the Somali Jet and pre-cursor disturbances from the W Pacific, in realistic representation of monsoon LPS. This was established using a series of regional climate models with different domains and forced with realistic boundary conditions from reanalysis. Improvements to the larger-scale monsoon circulation, in particular to the Somali Jet, with increased horizontal resolution are found, for example, due to improved representation of East African orography (Johnson et al 2016), again using older GA3 configuration global climate simulations. In addition, as some pre-cursor disturbances from the east originate from typhoons or tropical storms in the South China Sea or beyond (Saha et al 1981), it is likely that these are represented more accurately at higher resolution (Roberts et al. 2020), which will again improve conditions for Indian monsoon LPS to form.

The effect of coupling at higher resolution (GL_{90} - $ATM_{90}[GL]$) seems mostly to amplify these changes, with more LPS and associated rainfall over the central BoB and less to the north, which is associated with a southwards shift of the monsoon trough to a more realistic location away from the Himalayan foothills. This change in LPS rainfall again helps explain some of the changes seen in the mean seasonal rainfall due to coupling. In fact, locally over the BoB the changes in LPS rainfall account for (almost) all of the changes in the mean seasonal rainfall, as seen in Fig. 5 (note that values can exceed 100% due to compounding changes in mean rainfall from sources other than LPS). However, the main conclusion is that the effect of increasing resolution from 200km to 90km is far greater than that of air-sea coupling on Indian monsoon LPS.

With regards to changes in the effects of coupling as horizontal resolution is increased, these are much smaller than the effects of increasing resolution on its own. Therefore, the differences in effects of coupling at different resolutions are more than likely largely the result of the change in atmospheric monsoon base state between the 200km and 90km resolution simulations.

A comparison of the effects of coupling in individual basins at 90km (N216) horizontal resolution is shown in Figure 14. In general the number of LPS is substantially increased in all 90km (N216) experiments shown in Figure 14 compared to their 200km (N96) equivalents from Fig. 6. This further highlights that increasing the horizontal resolution from 200km (N96) to 90km (N216) dominates over the effects of air-sea coupling.

The positive effects from resolution and coupling combined, however, are still not quite as substantial as the improvements seen when the large-scale monsoon flow into South Asia is corrected, including the poten-

tial effects of precursor disturbances entering the monsoon region from the Western Pacific, in regional climate model atmosphere-only experiments (Levine and Martin, 2018). This suggests the biases in the atmospheric mean state and variability still inhibit the simulation of monsoon LPS.

3.4.2 Changes to wider area seasonal mean circulation

Seasonal means for Jun-Sept of air temperature at 850hPa and relative humidity at 500hPa are shown in Figure 9. Sufficiently high levels of mid-tropospheric humidity are considered to be an important factor in the genesis of monsoon LPS (e.g. Sikka 1977). Also, while there are no large differences in SST between $ATM_{200}[GL]$ / GL_{200} and $ATM_{90}[GL]$ / GL_{90} (see Fig. 2), differences in low-level air temperature may be an important factor in the formation and maintenance of the monsoon LPS.

In general the MetUM simulations are all too dry over most of India and its surrounding seas, with a seemingly large influence of dry and hot air from the continental area to the north west and the Arabian peninsula (see 850hPa air temperature field), with a particular lack of moisture availability over Indian land. There is improvement in available moisture and with higher resolution over the band covering the Arabian Sea, India and the Bay of Bengal, although there is still a remaining dry bias particularly over Indian land. The low-level air temperature anomalies are improved over the monsoon trough area at higher resolution. However, the persistent lack of available moisture over the land part of the monsoon trough would still act to inhibit systems from propagating westwards over India within the monsoon trough.

Note that in this case the free-running (atmosphere) climate model shows the opposite picture to that found in initialised NWP MetUM simulations by Hunt and Turner (2017), who find an overestimation of mid-level moisture availability in the monsoon trough and improvements as horizontal resolution is increased, indicating that outside/remote influences likely play a role in the simulations used in this study rather than simply being a local convection parametrisation issue.

The low-level circulation and precipitation are shown in Figure 10. Improvements in monsoon rainfall (and LPS rainfall) over India are also associated with an improvement to the excessive equatorial Indian Ocean convection at higher resolution. There are also clear increases in rainfall near bands of sharp (coastal) orography, such as the Western Ghats, Himalayas, and along the Myanmar coast, which are likely a direct result of the increase in resolution, that will contribute to

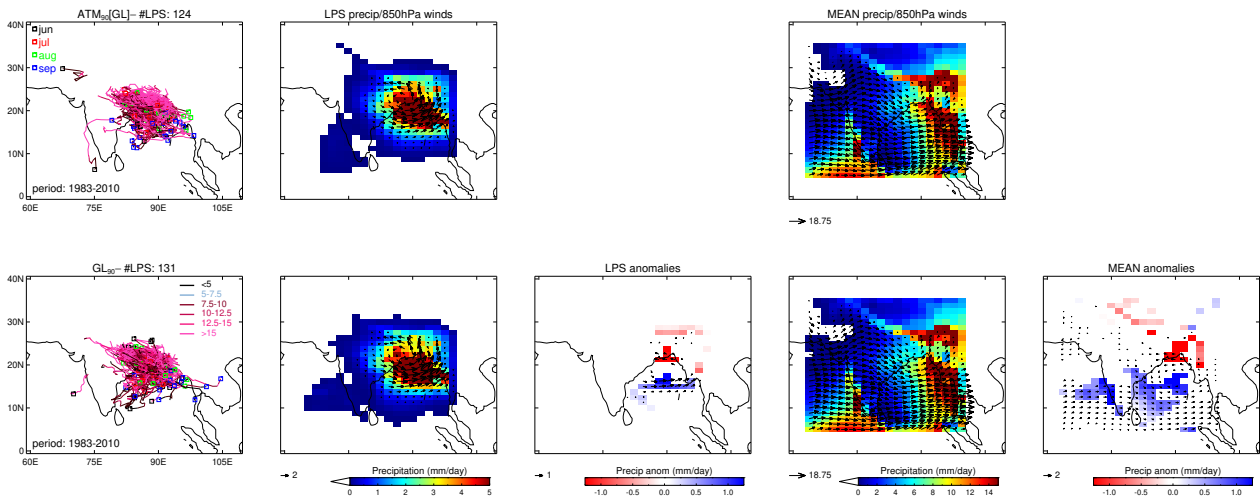


Fig. 8 Monsoon LPS diagnosed in 90km (N216) experiments for 1983-2010 period (only up to 2007 for re-analysis/observations). Top row shows the $ATM_{90}[GL]$ experiment, bottom row shows the GL_{90} experiment, with differences displayed as $[GL_{90} - ATM_{90}[GL]]$. The layout of the plots is as described in Fig. 4.

850 improved conditions over the Indian region. Further-
 851 more, correcting the inflow conditions into the Indian
 852 monsoon zone has been shown to substantially improve
 853 monsoon rainfall over India and also monsoon LPS (Levine
 854 and Martin 2018), therefore the dampening of equator-
 855 ial convection may play a role in the improvements to
 856 conditions over the Indian region, including the previ-
 857 ously discussed changes to moisture availability.

858 Upper level circulation fields and precipitation are
 859 shown in Figure 11. In addition to improvements to con-
 860 vection and upper-level divergence over the equatorial
 861 Indian Ocean there are similar improvements to exces-
 862 sive convection over the equatorial Atlantic Ocean with
 863 higher resolution. This could contribute to increases in
 864 Indian monsoon rainfall (Yadav 2017) and possibly pro-
 865 vide favourable conditions for monsoon LPS, although
 866 any definite impacts through this route require fur-
 867 ther investigation. There are also more complex changes
 868 across the Pacific, whose impact on the Indian monsoon
 869 is unclear and could be investigated.

870 The effects of air-sea coupling at higher resolution
 871 on the upper-level circulation and precipitation are shown
 872 in Figure 12. This shows the largest changes in convec-
 873 tion due to global coupling ($GL_{90} - ATM_{90}$) over the
 874 Indian and Pacific Ocean sectors, while changes over the
 875 equatorial Atlantic Ocean are relatively small. There
 876 are, however, some changes in the westerly jet across
 877 the North Atlantic which may feed into the cyclonic
 878 change in upper-level circulation to the north-west of
 879 India. If and precisely how this influences monsoon LPS
 880 also requires further investigation.

3.4.3 LPS intensity distribution, track and genesis density

881
 882
 883 Figure 13 shows further statistics for the globally cou-
 884 pled GOML2 experiments compared to their atmosphere-
 885 only equivalents. This shows that, once the role of reso-
 886 lution has been eliminated, ERA5 has more occurrences
 887 in the moderate intensities compared to all the model
 888 simulations, while the model simulations have some-
 889 what more occurrences at higher intensity. This is par-
 890 ticularly obvious when looking at the normalised fre-
 891 quency distributions. As well as more low- and mod-
 892 erate strength systems, this also reflects longer-lived
 893 strong systems in ERA5, while the systems in the model
 894 simulations initially have realistic intensity but are ter-
 895 minated too quickly, with many systems not travelling
 896 westwards across India in the monsoon trough.

897 The result for the 90km (N216) simulation is some-
 898 what similar to analysis by Hunt and Turner (2017, Fig.
 899 12a; note that their 200km (N96) to 90km (N216) jump
 900 is more dramatic) of MetUM initialised NWP simula-
 901 tions at different resolutions, although the analysis is
 902 slightly different in a number of factors. Firstly, Hunt
 903 and Turner (2017) use relative vorticity averaged over
 904 a cuboid of 400km surrounding the origin rather than
 905 the value at the centre of the tracked system at the
 906 850hPa level as used here. Furthermore, here: the re-
 907 sults have been filtered down to T42 resolution; LPS
 908 that are weaker than standard definitions for monsoon
 909 depressions are included in this study; here we use val-
 910 ues at the 850hPa single level instead of an average
 911 over 925-750hPa; and perhaps most significantly, the

simulations analysed here are free-running (in terms of atmosphere) climate simulations instead of initialised NWP simulations.

The track density and genesis show far more limited distributions of LPS in all model simulations compared to ERA5, with systems concentrated far too much over the northern Bay of Bengal. They appear to form in the correct location in the model simulations, but terminate too quickly after making landfall and therefore not enough systems traverse India westwards in the monsoon trough. This results in too little contribution to rainfall over Indian land.

3.4.4 Impact of air-sea coupling in individual basins at higher resolution

Analysing the impact of the effects of air-sea coupling in different areas at the higher resolution, the comparison is made using GL_{90} as the reference simulation. In this way we examine the contribution to the overall effect of global coupling from the following four areas:

1. **Coupling INSIDE Indian Ocean only:** $GL_{90} - AO_{PO_{90}}$ (Fig. 14, second row),
2. **Coupling OUTSIDE Indian Ocean:** $GL_{90} - IO_{90}$ (Fig. 14, third row),
3. **Coupling OUTSIDE Pacific Ocean:** $GL_{90} - PO_{90}$ (Fig. 14, fourth row),
4. **Coupling OUTSIDE Indian and Pacific Oceans:** $GL_{90} - IO_{PO_{90}}$ (Fig. 14, fifth row).

The inclusion of air-sea coupling inside the Indian Ocean ($GL_{90} - AO_{PO_{90}}$) shows a neutral impact on LPS numbers, unlike in the equivalent 200km (N96) simulations. There is though a similar, but smaller, positive impact on monsoon LPS rainfall over the BoB as found in the N96 simulations. The differences between the impacts at the two resolutions is seen clearer in Figure 15, which shows the $\Delta N_{216} - \Delta N_{96}$ (90km - 200km) double differences. However, at higher resolution there is also a small negative impact on monsoon LPS rainfall over northern India. This perhaps indicates a role for the negative local effect of air-sea coupling on LPS strength over the BoB, subsequently weakening the systems downstream as they move over land. Or this could be associated with a change in circulation over India.

The inclusion of air-sea coupling outside the Indian Ocean ($GL_{90} - IO_{90}$) shows a neutral impact both on LPS numbers and on the mean monsoon flow, again unlike the equivalent 200km (N96) simulation impact, while there is a small positive impact on LPS rainfall over the BoB. The impact on monsoon LPS rainfall is similar to effects of coupling inside the Indian Ocean

($GL_{90} - AO_{PO_{90}}$), suggesting again that the effects of coupling inside and outside the Indian Ocean have a similar impact on monsoon LPS. However, this impact is smaller than at 200km (N96) resolution.

Of the other areas shown, there is a much clearer positive effect compared to 200km (N96) on monsoon LPS rainfall, and consistent effects on the seasonal mean flow and rainfall, from the coupling outside the Indian and Pacific Ocean ($GL_{90} - IO_{PO_{90}}$), suggesting the Atlantic Ocean coupling has more influence at higher resolution. There is no obvious direct link between Atlantic Ocean coupled processes and monsoon LPS, though indirect links may include downstream effects of the Atlantic storm-track on the upper-level westerly flow over the Tibetan Plateau or changes in the MJO affecting the active/break cycles of the monsoon. While the larger-scale circulation changes in the 90km simulations due to global coupling are relatively small over the Atlantic Ocean (Fig. 12), there are some changes to the westerly jet across the North Atlantic which could merit further investigation.

The differences in the effects of coupling at the two different resolutions (Fig. 15) are relatively small for both coupling outside the Indian Ocean and coupling outside the Pacific Ocean, although highlight the greater reduction of mean JJAS Himalayan rainfall at higher resolution, which is part of the southwards shift of mean JJAS rainfall from the Himalayas seen at both resolutions. The last row of Fig. 15 highlights the increased LPS and mean rainfall at higher resolution with coupling outside the Indian and Pacific Ocean.

4 Discussion and Conclusions

The effects of air-sea coupling and horizontal resolution on the climate model simulation of monsoon LPS, which are important contributors to (extreme) Indian monsoon rainfall (Sikka 1977; Krishnamurthy and Ajayamohan 2010; Praveen et al. 2015; Hunt et al. 2016), are examined in order to understand the poor representation of LPS in current global climate models (Ashok et al. 2000; Sabre et al. 2000; Stowasser et al. 2009; Praveen et al. 2015, Levine and Martin 2018). While increasing horizontal resolution may be beneficial for capturing more detail, understanding the (combined) effects of air-sea coupling and horizontal resolution using current coupled models is hampered by the presence of widespread tropical SST biases. Therefore, in this study, we use climate simulations from MetUM-GOML2. This model couples the MetUM GA6 atmosphere to a mixed-layer ocean, which constrains the SSTs to observations, thereby minimising (but not eliminating) the effects of SST biases that are common in

many fully coupled atmosphere-ocean models. The robustness of the remaining SST biases between atmosphere-only MetUM-GOML2 simulations at different resolutions is evidence that this experimental approach ensures a consistent ocean mean state between resolutions, so that differences between the simulations can be attributed to differences in resolution only. Furthermore, while the atmospheric monsoon base state may be slightly different from the standard fully coupled and AMIP-style MetUM simulations, the isolated comparison of MetUM-GOML2 mixed-layer ocean coupled simulations and their equivalent atmosphere-only simulations (forced with GOML2 SSTs) does provide a cleaner decomposition into effects from coupling and from resolution.

Global coupling in the MetUM-GOML2 simulations ($GL - ATM[GL]$), when SST biases are excluded, has a neutral impact on the number of LPS formed, while the associated rainfall is somewhat reduced due to a negative air-sea feedback reducing the strength of atmospheric convection and weakening individual LPS, consistent with dampening effects on extreme tropical rainfall found by Hirons et al. (2018). When compared with a standard MetUM AMIP-type uncoupled run forced with observed SSTs, the MetUM-GOML2 global coupling results in larger numbers of LPS and associated rainfall, suggesting that the SST biases in MetUM-GOML2, though small, do play a role in altering the mean state of the monsoon. While this does not affect the MetUM-GOML2 global coupling ($GL - ATM[GL]$) comparison, it is relevant in the comparison of regionally coupled simulations, due to differences in SST in the uncoupled regions. This is due to differences in interannual SST variability, for example the uncoupled regions in MetUM-GOML2 coupled simulations are prescribed with climatological monthly-varying observed SST, and do not contain interannual variability. Furthermore, comparing coupled with uncoupled regions in the MetUM-GOML2 regionally coupled simulations is affected by the remaining SST biases developing in the coupled regions.

It is found that the regional simulations are particularly sensitive to localised coupling in the Indian and Pacific Oceans, which also has a positive effect on both the number of LPS and associated rainfall when compared with an uncoupled run forced with time-varying observed SSTs. As well as the direct effects of air-sea coupling in the individual oceans, this may also involve the aforementioned differences in SST, and in this case it seems likely that SST biases are at least partly responsible for the positive effects from Indian and Pacific Ocean coupling.

The remote effect of coupling within the Pacific Ocean may involve impacts on the Indian monsoon through the Walker circulation, or perhaps a change in the prevalence of westwards-travelling pre-cursor disturbances, which are thought to originate in the Western Pacific (Saha et al. 1981). These mechanisms have been suggested to affect the representation of monsoon LPS in regional climate model simulations (Levine and Martin, 2018). At higher resolution there is also an increased effect on LPS from coupling over the Atlantic Ocean. Further work is needed to properly establish the nature of these remote effects, which could also be the result of noise as only a single ensemble member is used in this study.

While global air-sea coupling, in the absence of SST biases, is shown to have a relatively small impact, it is found that increasing the horizontal resolution from N96 (200km) to N216 (90km) results in substantially larger improvements to both the simulation of Indian monsoon LPS and the mean state monsoon. Although the positive differences here are smaller than the benefits of eliminating remote biases, such as excessive equatorial Indian Ocean convection, observed in regional (atmosphere-only) climate model simulations (Levine and Martin, 2018), the effects of increasing resolution on LPS are found to be larger than in previous configurations of the MetUM (Johnson et al. 2016). While there are increased LPS numbers forming over the Bay of Bengal and increased LPS rainfall over north-eastern India in the higher resolution MetUM-GOML2 simulations, it is still found that the systems decay too soon after making landfall over India and many fail to continue westwards across India within the monsoon trough. This is consistent with the anomalously hot and dry conditions that prevail over Indian land and make for unfavourable conditions for LPS to be formed or maintained.

There are several factors that likely contribute to the improvements in LPS with increased horizontal resolution, including improved resolving of the structure of the LPS. This effect was seen using initialised NWP simulations of monsoon depressions using the same GA6 MetUM configuration by Hunt and Turner (2017), who found the greatest improvements when moving from N96 (denoted in this paper as 200km) to N216 (denoted in this paper as 90km), with little improvement beyond that. Improvements to the larger-scale circulation at higher resolution are also likely important, with Levine and Martin (2018) showing that improving the wider region circulation can have huge benefits to the representation of LPS. As discussed in previous sections, this probably relates to various factors, including dampening of excessive convection over the equatorial Indian

Ocean and changes to representation of orography, the latter of which is evident in rainfall changes near bands of sharp (coastal) mountains, and will contribute to improved conditions over the Indian region. Furthermore, there are possible improvements to pre-cursor disturbances from the W Pacific (Levine and Martin, 2018) that are sometimes linked to W Pacific typhoons or tropical storms making landfall (Saha et al 1981). This latter process may play a more prominent role at higher resolution due to improvements to tropical cyclone frequency and structure (Roberts et al. 2020). The new dynamical core ENDGAME included in the MetUM GA6 configuration used in this study enhances tropical variability, including tropical cyclone activity (Walters et al. 2017), and may play a role in the larger changes seen to the monsoon circulation with increased horizontal resolution compared to previous configurations (Johnson et al. 2016).

It is important to note that the methodology used in this study has some limitations, some of which are described in more detail in Hiron et al. (2015) and Peatman and Klingaman (2018): 1) The experiments are relatively short at approximately 30 years. While other studies using this GOML2 methodology (e.g. Peatman and Klingaman (2018)) have used simulations of similar length and found robust results for changes in seasonal mean and intraseasonal precipitation, longer simulations may confirm the findings presented here. 2) While the experiments using the MetUM-GOML2 framework allow a relatively pure comparison of effects of air-sea coupling and resolution, the atmospheric base state is a little different to the standard MetUM AMIP-style simulations, mainly due to remaining cold SST biases (which are still relatively small compared to the fully coupled MetUM), the effects of which require further investigation. 3) In terms of the coupling, the lack of ocean dynamics in the MetUM-GOML2 model means there is no representation of ENSO or IOD variability in the ocean (Hiron et al. 2015). This may be important if there are non-linear effects of ENSO and IOD variability on the number of LPS and their associated rainfall. 4) The uncoupled regions of the regionally coupled simulation are forced with climatological monthly-varying observed SST, which introduces differences in interannual SST variability compared to the globally coupled simulation and the atmosphere-only (AMIP-type) simulation forced with time-varying observed SST. Furthermore, the uncoupled regions do not include any SST biases or interannual variability present in those regions in the atmosphere-only simulation forced with SSTs from the globally coupled simulation. 5) The current study has only tested two horizontal resolutions. 6) The MetUM atmosphere model used has an inherent

strong mean dry bias in Indian monsoon rainfall (part of which involves the lack of LPS and associated rainfall, which is also associated with the limited westwards progression over Indian land of these systems).

It is possible that all these factors may influence the results. For example, the positive effects from resolution and coupling combined are still not quite as substantial as the improvements seen when the large-scale monsoon flow into South Asia is corrected (Levine and Martin, 2018), which suggests that the inherent MetUM biases in the atmospheric mean state and variability still inhibit the simulation of monsoon LPS. Using other models that have different mean biases and/or moving to higher horizontal resolutions than used here ($< 90\text{km}$) may show different sensitivities, although it is worth noting that Hunt and Turner (2017) found little improvements in MetUM NWP case studies of monsoon depressions when resolution was increased beyond 63-39km. The limitations discussed here require further attention in subsequent investigations.

Acknowledgements This work and its contributors (Richard Levine and Gill Martin) was supported through the Weather and Climate Science for Service Partnership (WCSSP) India, a collaborative initiative between the Met Office, supported by the UK Government's Newton Fund, and the Indian Ministry of Earth Sciences (MoES). Nicholas Klingaman was supported by an Independent Research Fellowship from the Natural Environment Research Council (NE/L010976/1) and by the NERC/Global Challenges Research Fund programme Atmospheric hazards in developing countries: risk assessment and early warnings (ACREW). Simon Peatman was supported by the NERC Bay of Bengal Boundary Layer Experiment project of the (NE/L013800/1). ERA5 figures in this paper have been generated using Copernicus Climate Change Service Information 2020. The authors would like to thank the two anonymous reviewers for suggestions that helped improve the manuscript.

References

- Adler RF, Huffman GJ, Chang A, Ferraro R, Xie PP, Janowiak J, Rudolf B, Schneider U, Curtis S, Bolvin D, Gruber A, Susskind J, Arkin P, Nelkin E (2003). The version-2 global precipitation climatology project (GPCP) monthly precipitation analysis (1979–present). *J Clim* 4:1147–1167
- Ashok K, Soman MK, Satyan V (2000). Simulation of monsoon disturbances in a GCM. *Pure Appl Geophys* 157:1509–1539. 2000
- Bollasina M and Nigam S (2009). Indian Ocean SST, evaporation, and precipitation during the South Asian summer monsoon in IPCC-AR4 coupled simulations. *Clim Dyn* 33: 1017. <https://doi.org/10.1007/s00382-008-0477-4>
- Bollasina MA, Ming Y (2013). The general circulation model precipitation bias over the southwestern equatorial Indian Ocean and its implications for simulating the South Asian monsoon. *Clim Dyn* 40: 823–838. <https://doi.org/10.1007/s00382-012-1347-7>

5. Copernicus Climate Change Service (C3S) (2017): ERA5: Fifth generation of ECMWF atmospheric re-analyses of the global climate. Copernicus Climate Change Service Climate Data Store (CDS), 2020. <https://cds.climate.copernicus.eu/cdsapp#!/home>
6. DeMott CA, Stan C, Randall DA, Branson MD (2014). Intraseasonal variability in coupled GCMs: The roles of ocean feedbacks and model physics. *J Clim* 27: 4970–4995. <https://doi.org/10.1175/JCLI-D-13-00760.1>
7. DeMott CA, Klingaman NP, Woolnough SJ (2015). Atmosphere-Ocean Coupled Processes in the Madden-Julian Oscillation. *Rev Geophys* 53: 1099–1154. <https://doi.org/10.1002/2014RG000478>
8. Fu X and Wang B (2004). Differences of boreal summer intraseasonal oscillations simulated in an atmosphere-ocean coupled model and an atmosphere-only model. *J Clim* 17: 1263–1271. [https://doi.org/10.1175/1520-0442\(2004\)017<1263:DOBSIO>2.0.CO;2](https://doi.org/10.1175/1520-0442(2004)017<1263:DOBSIO>2.0.CO;2)
9. Gao Y, Klingaman NP, DeMott CA, Hsu P-C (2019). Diagnosing ocean feedbacks to the BSISO: SST-modulated surface fluxes and the moist static energy budget. *J Geophys Res Atmos* 124: 146–170. <https://doi.org/10.1029/2018JD029303>
10. Gates WL et al. (1998). An Overview of the Results of the Atmospheric Model Intercomparison Project (AMIP I). *Bull Amer Meteor Soc* 73: 1962–1970.
11. Halkides DJ, Waliser DE, Lee T, Nemenlis D, Guan B (2015). Quantifying the processes controlling intraseasonal mixed-layer temperature variability in the tropical Indian Ocean. *J Geophys Res Oceans* 120: 692–715. <https://doi.org/10.1002/2014JC010139>
12. Hirons LC, Klingaman NP, Woolnough SJ (2015). MetUM-GOML1: a near-globally coupled atmosphere-ocean-mixed-layer model. *Geosci Model Dev* 8: 363–379, 2015. <https://doi.org/10.5194/gmd-8-363-2015>
13. Hirons LC, Klingaman NP, Woolnough SJ (2018). The impact of air-sea interactions on the representation of tropical precipitation extremes. *J Adv Model Earth Sy* 10: 550–559. <https://doi.org/10.1002/2017MS001252>
14. Hodges KI (1994). A general method for tracking analysis and its application to meteorological data. *Mon Weather Rev* 122:2573–2586
15. Hsu W-C, Patricola M, Chang P (2019). The impact of climate model sea surface temperature biases on tropical cyclone simulations. *Clim Dyn* 53(1-2): 173–192. <https://doi.org/10.1007/s00382-018-4577-5>
16. Hunt KMR, Turner AG, Inness PM, Parker DE, Levine RC (2016). On the structure and dynamics of Indian monsoon depressions. *Mon Weather Rev* 144(9): 3391–3416. <https://doi.org/10.1175/MWR-D-15-0138.1>
17. Hunt KMR and Turner AG (2017). The effect of horizontal resolution on Indian monsoon depressions in the Met Office NWP model. *Q J R Meteorol Soc*. <https://doi.org/10.1002/qj.3030>
18. Johnson SJ, Levine RC, Turner AG, Martin GM, Woolnough SJ, Schiemann R, Mizieliński MS, Roberts MJ, Vidale PL, Demory M-E, Strachan J (2016). The resolution sensitivity of the South Asian Monsoon and Indo-Pacific in a global 0.35 degree AGCM. *Clim Dynam*. 46: 807. <https://doi.org/10.1007/s00382-015-2614-1>
19. Karmacharya J, Levine RC, Jones R, Moufouma-Okia W, New M (2015). Sensitivity of systematic biases in South Asian summer monsoon simulations to regional climate model domain size and implications for downscaled regional process studies. *Clim Dynam*. 45(1-2):213–231. <https://doi.org/10.1007/s00382-015-2565-6>
20. Karmacharya J, New M, Jones R, Levine R (2016). Added value of a high resolution regional climate model in simulation of intraseasonal variability of the South Asian summer monsoon. *Int J Climatol*. <https://doi.org/10.1002/joc.4767>
21. Klingaman NP and Woolnough SJ (2014). The role of air-sea coupling in the simulation of the Madden-Julian oscillation in the Hadley Centre model. *Q J Roy Meteor Soc* 140:2272–2286. <https://doi.org/10.1002/qj.2295>
22. Krishnamurthy V and Shukla J (2007). Intraseasonal and seasonally persisting patterns of Indian monsoon rainfall. *J Clim* 20:3–20. <https://doi.org/10.1175/JCLI3981.1>
23. Krishnamurthy V and Ajayamohan RS (2010). Composite Structure of Monsoon Low Pressure Systems and Its Relation to Indian Rainfall. *J Clim*. 23-4285-4305. <https://doi.org/10.1175/2010JCLI2953.1>
24. Levine RC and Martin GM (2018). On the climate model simulation of Indian monsoon low pressure systems and the effect of remote disturbances and systematic biases. *Clim Dynam* 50(11-12):4721-4743. <https://doi.org/10.1007/s00382-017-3900-x>
25. Levine RC, Turner AG, Marathayil D, Martin GM (2013). The role of northern Arabian Sea surface temperature biases in CMIP5 model simulations and future projections of Indian summer monsoon rainfall. *Clim Dyn* 41: 155–172. <https://doi.org/10.1007/s00382-012-1656-x>
26. Levine RC, Turner AG (2012). Dependence of Indian monsoon rainfall on moisture fluxes across the AS and the impact of coupled model sea surface temperature biases. *Clim Dynam* 38(11-12):2167-2190. <https://doi.org/10.1007/s00382-011-1096-z>
27. Peatman SC and Klingaman NP (2018). The Indian summer monsoon in MetUM-GOML2.0: effects of air-sea coupling and resolution. *Geosci Model Dev* 11:4693-4709. <https://doi.org/10.5194/gmd-11-4693-2018>
28. Praveen V, Sandeep S, Ajayamohan RS (2015). On the Relationship between Mean Monsoon Precipitation and Low Pressure Systems in Climate Model Simulations. *J Clim* 28:5305-5324. <https://doi.org/10.1175/JCLI-D-14-00415.1>
29. Prodhomme C, Terray P, Masson S et al. (2014). Impacts of Indian Ocean SST biases on the Indian Monsoon: as simulated in a global coupled model. *Clim Dyn* 42: 271–290. <https://doi.org/10.1007/s00382-013-1671-6>
30. Reynolds RW, Smith TM, Liu C, Chelton DB, Casey KS, Schlax MG (2007) Daily high-resolution-blended analyses for sea surface temperature. *J Clim* 20:5473–5496. <https://doi.org/10.1175/2007JCLI1824.1>
31. Roberts MJ et al. (2020). Impact of Model Resolution on Tropical Cyclone Simulation Using the High-ResMIP-PRIMAVERA Multimodel Ensemble. *J Clim* 33: 2557–2583. <https://doi.org/10.1175/JCLI-D-19-0639.1>
32. Sabre M, Hodges KI, Laval K, Polcher J, Desalmand F (2000). Simulation of monsoon disturbances in the LMD GCM. *Mon Weather Rev* 128:3752–3771
33. Saha K, Sanders F, Shukla J (1981). Westward Propagating Predecessors of Monsoon Depressions. *Mon Weather Rev*. 109:330-343. [https://doi.org/10.1175/1520-0493\(1981\)109<0330:WPPOMD>2.0.CO;2](https://doi.org/10.1175/1520-0493(1981)109<0330:WPPOMD>2.0.CO;2)
34. Shukla RP, Huang B (2016). Interannual variability of the Indian summer monsoon associated with the air-sea feedback in the northern Indian Ocean. *Clim Dyn* 46: 1977–1990. <https://doi.org/10.1007/s00382-015-2687-x>
35. Sikka DR (1977). Some aspects of the life history, structure and movement of monsoon depressions. *Pure Appl Geophys*. 115:1501–1529

- 1359 36. Smith DM, Murphy JM (2007). An objective ocean tem-
1360 perature and salinity analysis using covariances from a
1361 global climate model. *J Geophys Res Ocean* 112 (C02022).
1362 <https://doi.org/10.1029/2005JC003172>
- 1363 37. Stowasser M, Annamalai H, Hafner J (2009). Response
1364 of the South Asian summer monsoon to global warm-
1365 ing; mean and synoptic systems. *J Clim* 22:1014–1036.
1366 <https://doi.org/10.1175/2008JCLI2218.1>
- 1367 38. Subrahmanyam B, Murty VSN, Sharp RJ, O'Brien
1368 JJ (2005). Air-sea Coupling During the Tropical Cy-
1369 clones in the Indian Ocean: A Case Study Using Satel-
1370 lite Observations. *Pure appl geophys* 162: 1643-1672.
1371 <https://doi.org/10.1007/s00024-005-2687-6>
- 1372 39. Wainwright CM, Hiron LC, Klingaman NP, Allan RP,
1373 Black E, Turner AG (2019) The impact of air-sea cou-
1374 pling and ocean biases on the seasonal cycle of south-
1375 ern West African precipitation. *Clim Dyn* 53: 7027–7044.
1376 <https://doi.org/10.1007/s00382-019-04973-0>
- 1377 40. Walters DN et al. (2011). The Met Office Unified
1378 Model Global Atmosphere 6.0/6.1 and JULES Global
1379 Land 3.0/3.1 configurations. *Geosci Model Dev* 4: 919–941.
1380 <https://doi.org/10.5194/gmd-4-919-2011>
- 1381 41. Walters DN et al. (2017). The Met Office Unified
1382 Model Global Atmosphere 6.0/6.1 and JULES Global Land
1383 6.0/6.1 configurations. *Geosci Model Dev* 10(4), 1487-1520.
1384 <https://doi.org/10.5194/gmd-10-1487-2017>
- 1385 42. Williams KD et al. (2015). The Met Office Global Cou-
1386 pled model 2.0 (GC2) configuration. *Geosci Model Dev* 8:
1387 1509–1524. <https://doi.org/10.5194/gmd-8-1509-2015>
- 1388 43. Wu G, Guan Y, Liu Y, Yan J, Mao J (2012). Air-sea
1389 interaction and formation of the Asian summer monsoon
1390 onset vortex over the Bay of Bengal. *Clim Dyn* 38(1-2):
1391 261-279. <https://doi.org/10.1007/s00382-010-0978-9>
- 1392 44. Yadav RK (2017). On the relationship between east
1393 equatorial Atlantic SST and ISM through Eurasian wave.
1394 *Clim Dyn* 48: 281–295. [https://doi.org/10.1007/s00382-](https://doi.org/10.1007/s00382-016-3074-y)
1395 [016-3074-y](https://doi.org/10.1007/s00382-016-3074-y)
- 1396 45. Yatagai A, Kamiguchi K, Arakawa O, Hamada A, Ya-
1397 sutomi N, Kitoh A (2012). APHRODITE: Constructing a
1398 Long-Term Daily Gridded Precipitation Dataset for Asia
1399 Based on a Dense Network of Rain Gauges. *BAMS*. Septem-
1400 ber 2012:1401-1415

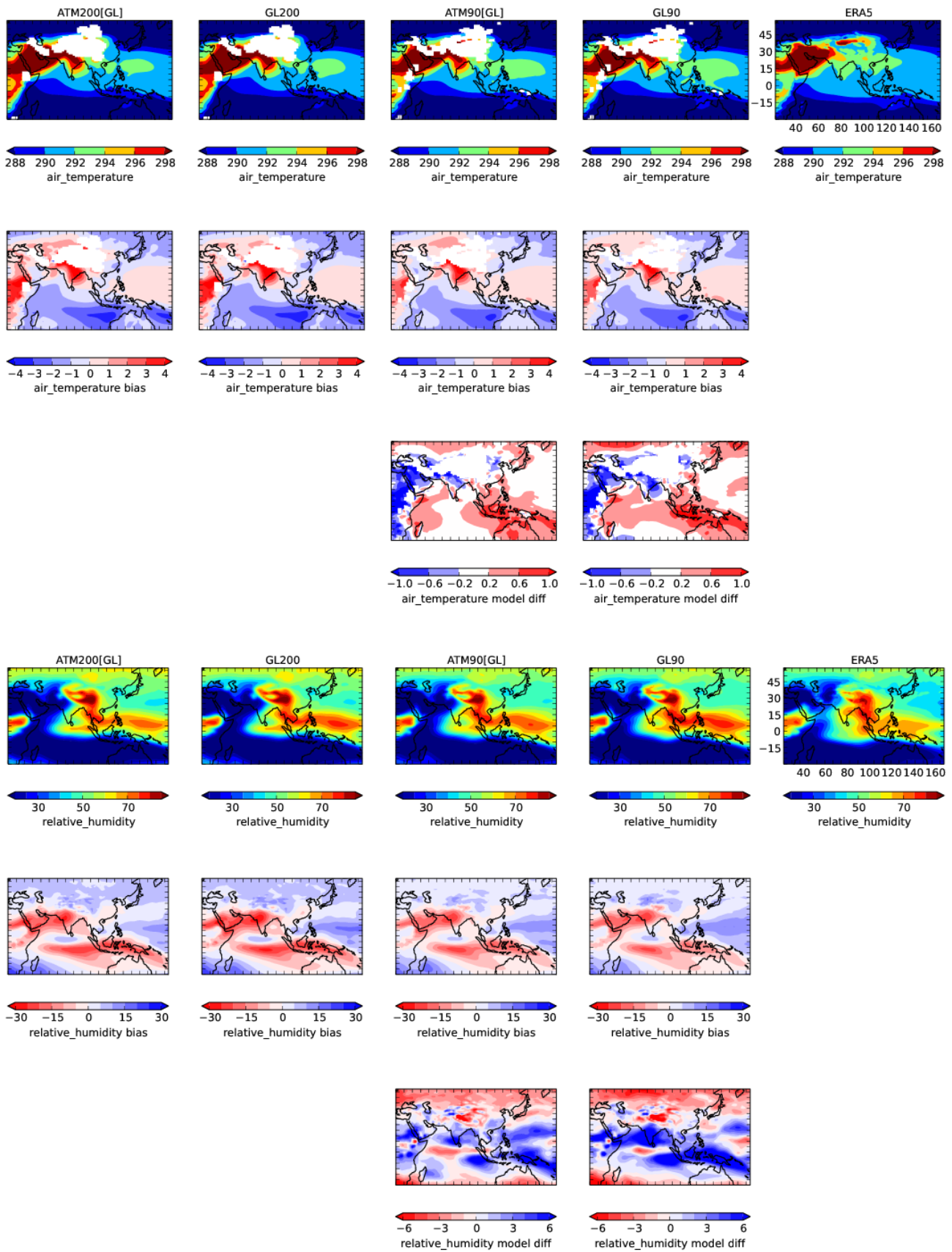


Fig. 9 Row (1) Air temperature (in K, average for Jun-Sept) at 850hPa. Row (2) Differences compared to ERA5. Row (3) 90km minus 200km ($ATM_{90}[GL] - ATM_{200}[GL]$ and $GL_{90} - GL_{200}$) and relative humidity (in %, average for Jun-Sept) at 500hPa for Jun-Sept and differences compared to ERA5 in same layout as for air temperature. Seasonal Jun-Sept means for the period 1983-2010. The ERA5 figures have been generated using Copernicus Climate Change Service Information 2020.

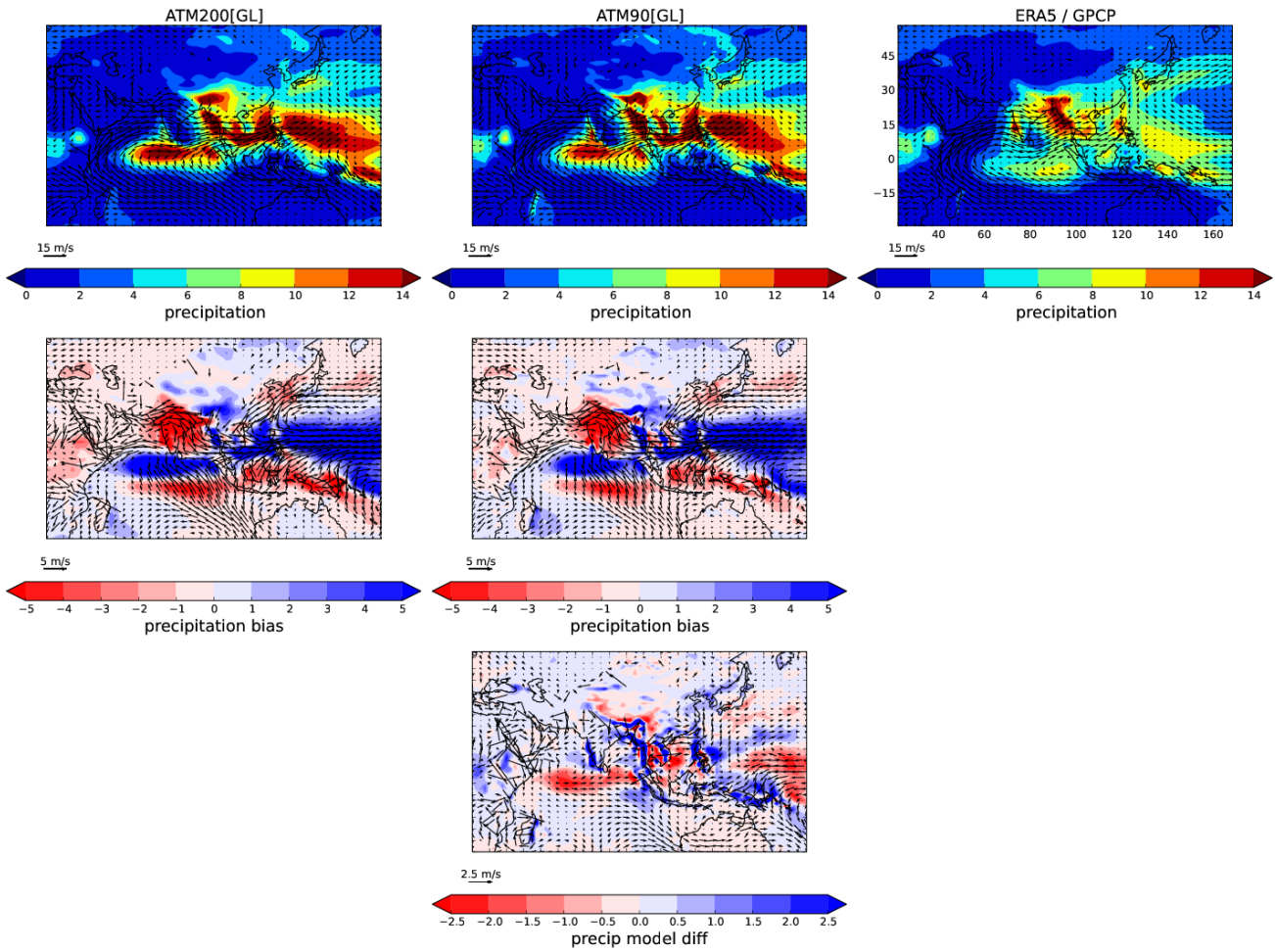


Fig. 10 Row (1) Precipitation (mm/day, coloured contours) and 850hPa winds (m/s, vectors). Row (2) Differences compared to ERA5 and GPCP precipitation. Row (3) 90km minus 200km ($ATM_{90}[GL] - ATM_{200}[GL]$). Seasonal Jun-Sept means for the period 1983-2010. The ERA5 figures have been generated using Copernicus Climate Change Service Information 2020.

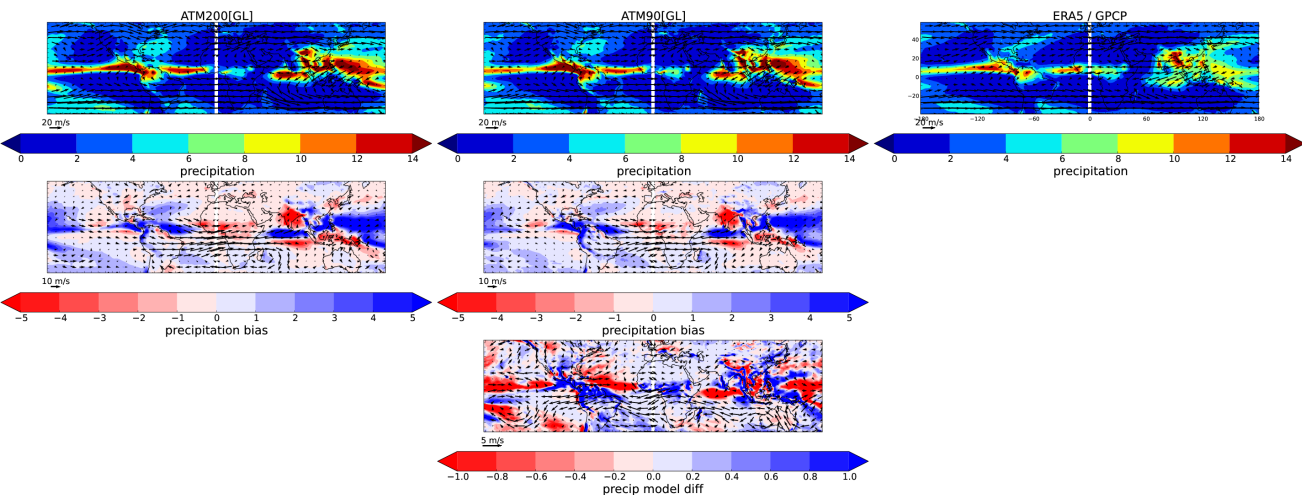


Fig. 11 Row (1) Precipitation (mm/day, coloured contours) and 200hPa winds (m/s, vectors). Row (2) Differences compared to ERA5 and GPCP precipitation. Row (3) 90km minus 200km ($ATM_{90}[GL] - ATM_{200}[GL]$). Seasonal Jun-Sept means for the period 1983-2010. The ERA5 figures have been generated using Copernicus Climate Change Service Information 2020.

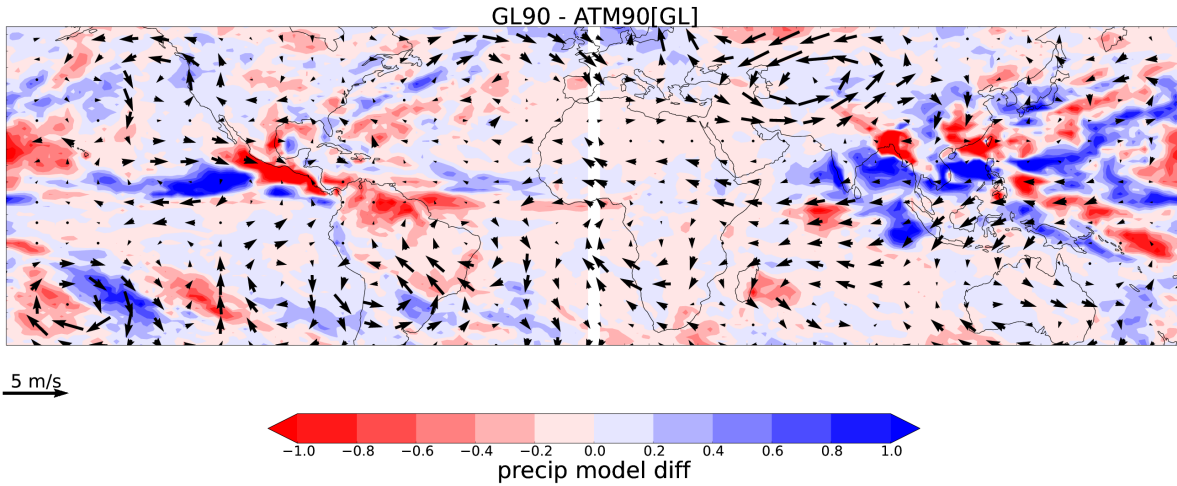


Fig. 12 Differences in precipitation (mm/day, coloured contours) and 200hPa winds (m/s, vectors) for global coupling minus atmosphere-only simulations at 90km ($GL_{90}[GL] - ATM_{90}[GL]$). Seasonal Jun-Sept mean for the period 1983-2010.

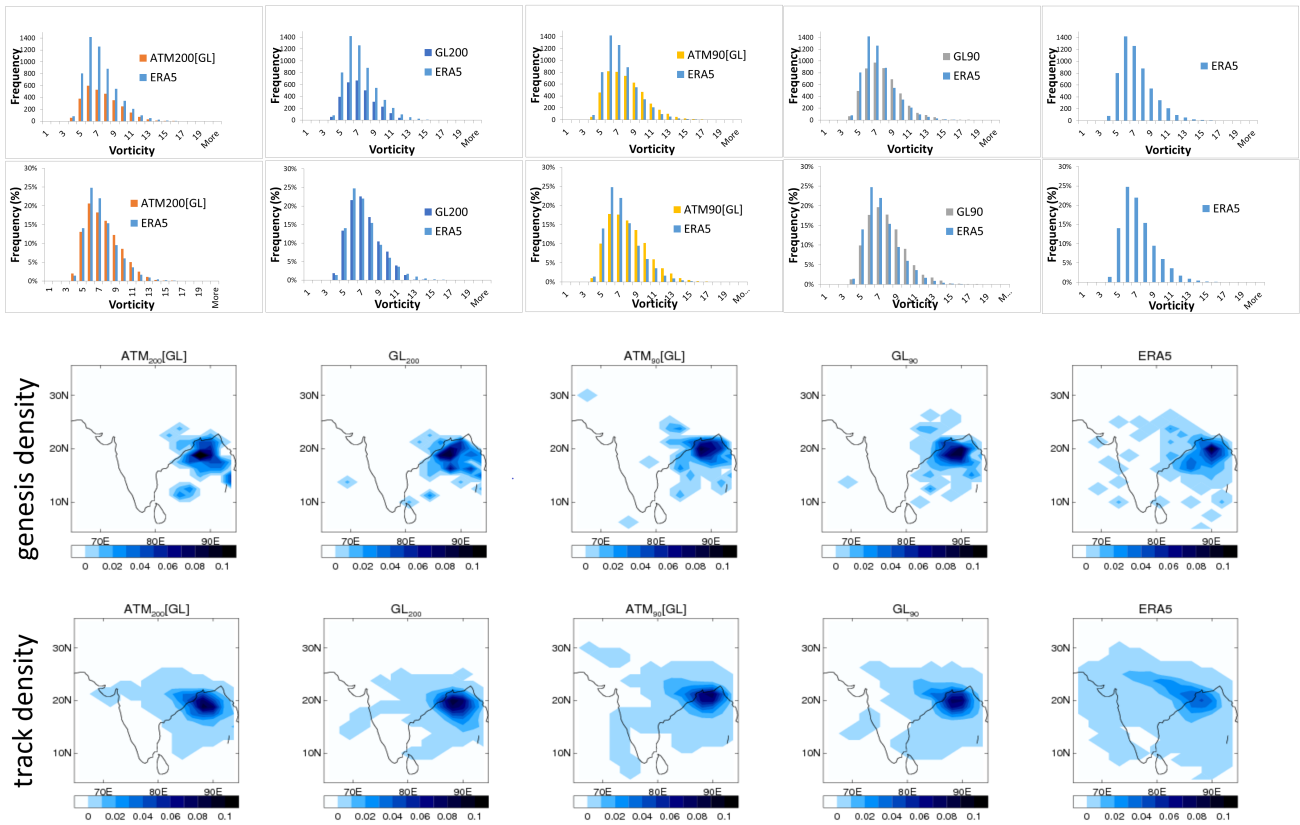


Fig. 13 LPS intensity histograms (as described in Fig. 1). First row is total occurrences, second row is normalised frequency distribution, third row is LPS track genesis (from equation 2), fourth row is LPS track density (from equation 1). The columns show experiments $ATM_{200}[GL]$, GL_{200} , $ATM_{90}[GL]$, GL_{90} , $ERA5$. The ERA5 figures have been generated using Copernicus Climate Change Service Information 2020.

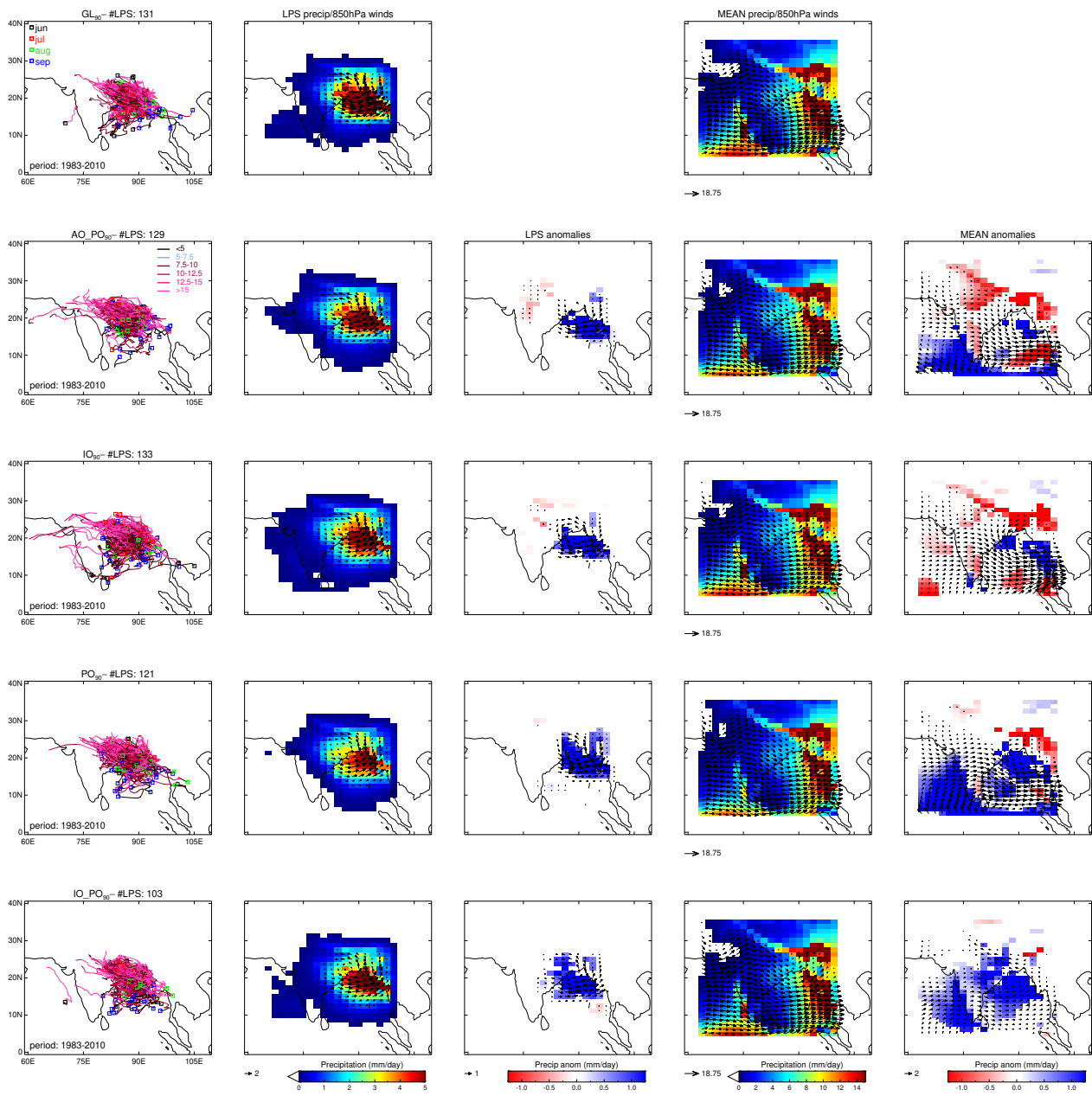


Fig. 14 Coupling sensitivity of 90km (N216) simulations for 1983-2010 period. Top row shows the Global Coupling (obs) experiment, while subsequent rows show the results for regional coupling and differences displayed as $[GL_{90} - AO_{PO_{90}}]$ (coupling INSIDE Indian Ocean), $[GL_{90} - IO_{90}]$ (coupling OUTSIDE Indian Ocean), $[GL_{90} - PO_{90}]$ (coupling OUTSIDE Pacific Ocean), $[GL_{90} - IO_{PO_{90}}]$ (coupling OUTSIDE Indian and Pacific Oceans). The layout of the plots is as described in Fig. 4.

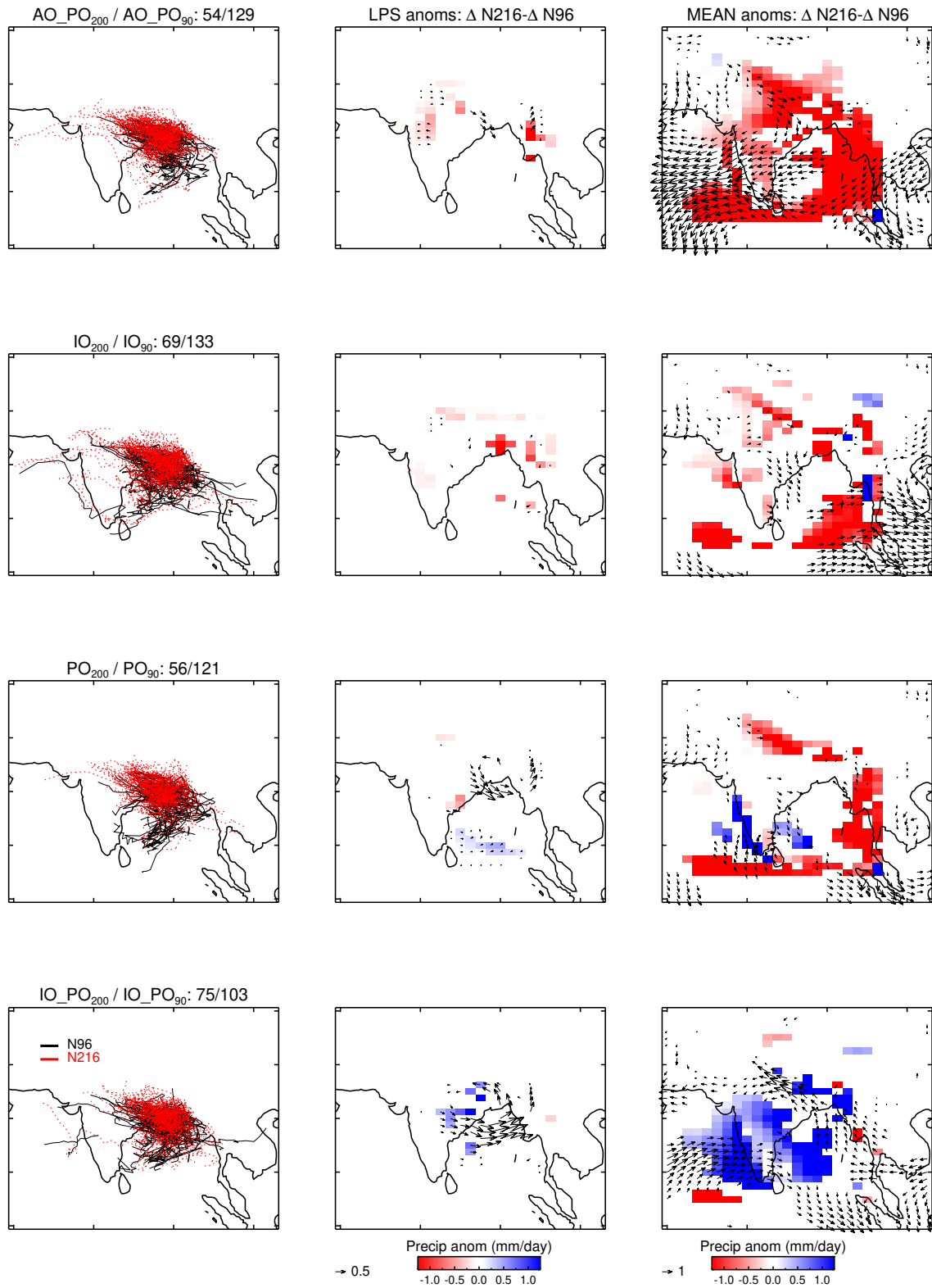


Fig. 15 Comparison of coupling sensitivity for coupling experiments (EXPT) at 90km (N216) versus 200km (N96) simulations for 1983-2010 period in terms of double differences: $\Delta N216 - \Delta N96 = (GL_{90} - EXPT_{90}) - (GL_{200} - EXPT_{200})$. The *first panel on left hand-side* shows LPS trajectories with the total number of LPS in title for N96 (black) and N216 (red dotted). The *second panel from left* shows double differences in LPS contribution to Jun-Sept seasonal mean precipitation (mm/day) and 850 hPa winds (m/s, black vectors). The *third panel from left* shows double differences Jun-Sept seasonal mean precipitation (mm/day) and 850hPa wind (m/s) contributions. All data in panels two and three are plotted on a common 200km (N96; $1.875^\circ \times 1.25^\circ$) grid. Only significant differences and vectors at 90% level using a student t-test are shown. Values exceeding the colour scale maxima are capped at the relevant maximum colour value.